Neuron

Article

Glutamate in primary afferents is required for itch transmission

Highlights

- Itch-selective MRGPRA3$^+$ afferents highly express *Vglut2* and *Nmb*
- Glutamate is an essential neurotransmitter in MRGPRA3$^+$ afferents for itch signaling
- MRGPRA3$^+$ afferents form monosynaptic connections with NMBR$^+$ dorsal horn neurons
- *Nmb* in MRGPRA3$^+$ afferents and NMBR$^+$ dorsal horn neurons function in itch sensation

Authors

Lian Cui, Jeff Guo, Suna L. Cranfill, ..., Minghong Ma, Qin Liu, Wenqin Luo

Correspondence

qinliu@wustl.edu (Q.L.), luow@pennmedicine.upenn.edu (W.L.)

In brief

Cui et al. demonstrate that glutamate is required for itch transmission in MRGPRA3$^+$ primary afferents, which also use the neuropeptide NMB to enhance signaling. Because both glutamate and *Nmb* are broadly available in primary afferents, this suggests that distinct neurotransmitters are not necessary to confer itch modality specificity.

Cui et al., 2022, Neuron *110*, 809–823
March 2, 2022
https://doi.org/10.1016/j.neuron.2021.12.007

CellPress

Neuron

CellPress

Article

Glutamate in primary afferents is required for itch transmission

Lian Cui,[1] Jeff Guo,[2,6] Suna L. Cranfill,[1,6] Mayank Gautam,[1] Janardhan Bhattarai,[1] William Olson,[3] Katherine Beattie,[1] Rosemary C. Challis,[4] Qinxue Wu,[1] Xue Song,[1] Tobias Raabe,[5] Viviana Gradinaru,[4] Minghong Ma,[1] Qin Liu,[2,*] and Wenqin Luo[1,7,*]

[1]Department of Neuroscience, Perelman School of Medicine, University of Pennsylvania, Philadelphia, PA 19104, USA
[2]Department of Anesthesiology, Center for the Study of Itch, Washington University School of Medicine in St. Louis, St. Louis, MO 63110, USA
[3]Department of Neuroscience, Johns Hopkins University School of Medicine, Baltimore, MD 21205, USA
[4]Division of Biology and Biological Engineering, California Institute of Technology, Pasadena, CA 91125, USA
[5]Division of Translational Medicine and Human Genetics, Perelman School of Medicine, University of Pennsylvania, Philadelphia, PA 19104, USA
[6]These authors contributed equally
[7]Lead contact
*Correspondence: qinliu@wustl.edu (Q.L.), luow@pennmedicine.upenn.edu (W.L.)
https://doi.org/10.1016/j.neuron.2021.12.007

SUMMARY

Whether glutamate or itch-selective neurotransmitters are used to confer itch specificity is still under debate. We focused on an itch-selective population of primary afferents expressing MRGPRA3, which highly expresses *Vglut2* and the neuropeptide neuromedin B (*Nmb*), to investigate this question. Optogenetic stimulation of MRGPRA3$^+$ afferents triggers scratching and other itch-related avoidance behaviors. Using a combination of optogenetics, spinal cord slice recordings, *Vglut2* conditional knockout mice, and behavior assays, we showed that glutamate is essential for MRGPRA3$^+$ afferents to transmit itch. We further demonstrated that MRGPRA3$^+$ afferents form monosynaptic connections with both NMBR$^+$ and NMBR$^-$ neurons and that NMB and glutamate together can enhance the activity of NMBR$^+$ spinal DH neurons. Moreover, *Nmb* in MRGPRA3$^+$ afferents and NMBR$^+$ DH neurons are required for chloroquine-induced scratching. Together, our results establish a new model in which glutamate is an essential neurotransmitter in primary afferents for itch transmission, whereas NMB signaling enhances its activities.

INTRODUCTION

Itch is an unpleasant sensation that triggers a desire to scratch (Ikoma et al., 2006). Acute itch alerts an organism to harmful external threats, whereas chronic itch is a debilitating disorder that can cause skin excoriations and lead to sleep deprivation, anxiety, and depression (Pereira and Stander, 2017; Ständer et al., 2007). Pruritogenic stimuli are detected by primary somatosensory neurons in the dorsal root ganglia (DRG) and trigeminal ganglia (TG), which synapse with spinal cord or medulla dorsal horn (DH) interneurons (Bautista et al., 2014; Dong and Dong, 2018). Spinal cord or medulla DH neurons then integrate and relay itch information to various brain regions. A family of G protein-coupled receptors (GPCRs), Mas-related G protein-coupled receptors (MRGPRs), encodes receptors for itch-inducing substances (Liu et al., 2009). For example, MRGPRA3 is activated by chloroquine (CQ), an antimalarial drug that causes itch as a side effect (Mnyika and Kihamia, 1991). MRGPRA3$^+$ afferents form a population of "itch-selective" afferents that are both necessary and sufficient for itch sensation, as demonstrated by ablation and activation studies using *Mrgpra3*^{Cre} transgenic mice (Han et al., 2013; Sun et al., 2017).

Because the gross anatomy of itch-sensitive and nociceptive afferents is similar, how these two neural pathways generate distinct perceptions and behaviors is an unresolved question. One proposed model, the "itch-selective neurotransmitter" model, suggests that itch afferents use selective neurotransmitters, specifically neuropeptides, such as gastrin-releasing peptide (GRP) or brain natriuretic peptide (BNP or NPPB), to communicate with downstream DH neurons (Ma, 2014; Mishra and Hoon, 2013; Sun et al., 2009). Glutamate, on the other hand, has been proposed to be dispensable for this function (Chen and Sun, 2020; Lagerström et al., 2010; Liu et al., 2010; Ma, 2014). This model is supported by experimental results: (1) transcripts of these neuropeptide genes are expressed in rodent DRG neurons, whereas their respective receptors (GRPR and NPRA) show complementary expression in spinal cord DH neurons (Carstens, 2016; Carstens et al., 2010; Fleming et al., 2012; Mishra and Hoon, 2013; Sun and Chen, 2007; Sun et al., 2009); (2) intrathecal injection of these neuropeptides causes scratching (i.e., itch behavior) in rodents (Mishra et al., 2012; Su and

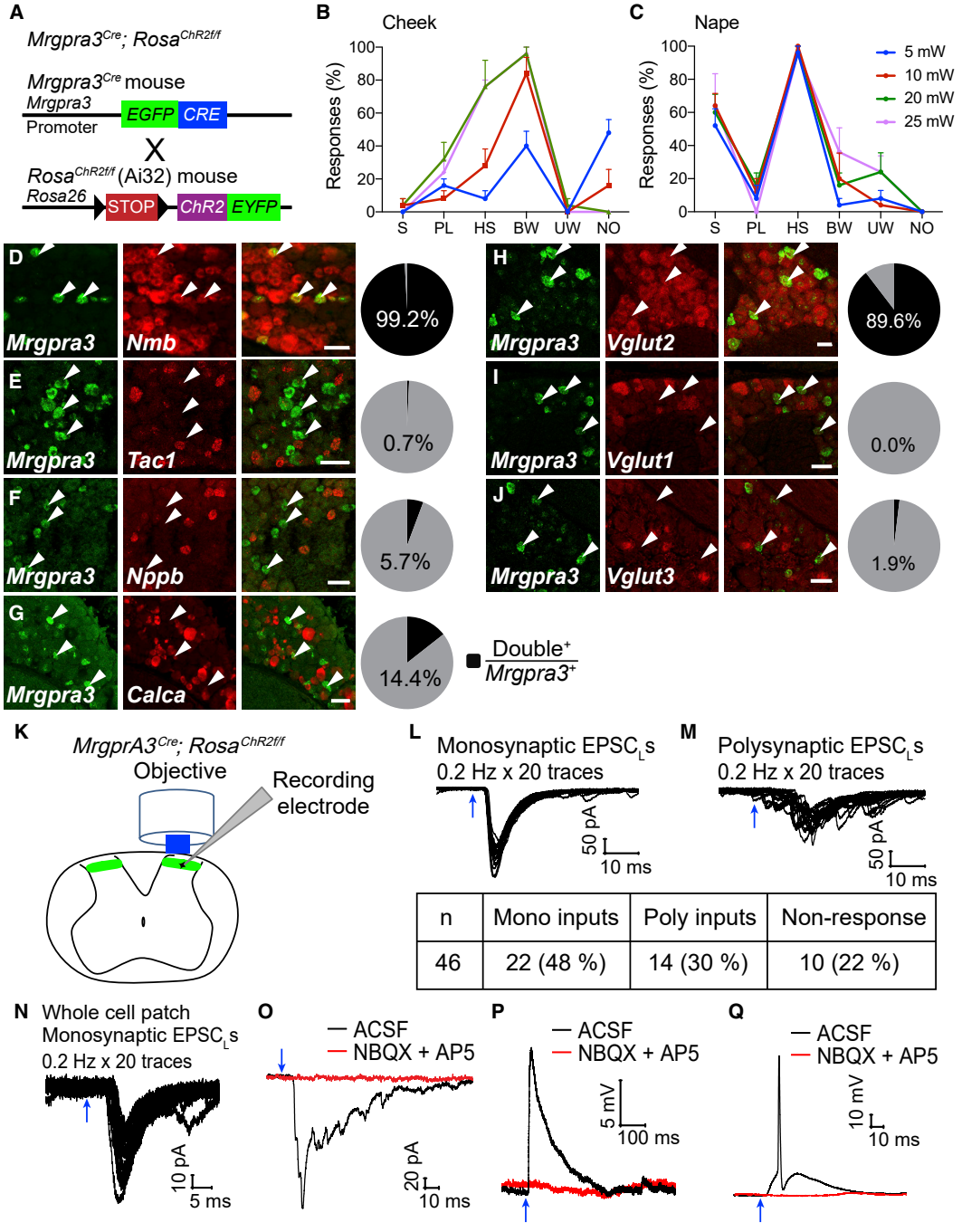

Figure 1. Optical stimulation of *Mrgpra3-ChR2* mice triggers itch-related behaviors, and *Nmb* and *Vglut2* are highly expressed in *Mrgpra3*$^{+}$ DRG neurons

(A) Diagram showing genomic structure of *Mrgpra3*^{cre}; *Rosa*$^{ChR2f/f}$ mice.

(B and C) The percentage of *Mrgpra3-ChR2* mouse behaviors in response to different intensities of blue laser stimuli at the cheek or nape of the neck, including scratching (S), ipsilateral paw lifting (PL), head shaking (HS), grooming (G), wiping (W), or no response (NO). Each dot indicates one animal. 10 trials per 6-month-old mouse, n = 5.

(legend continued on next page)

Ko, 2011; Sun and Chen, 2007), whereas genetic ablation of *Grpr* or toxin-mediated ablation of GRPR$^+$ or NPRA$^+$ neurons leads to a selective reduction in itch-related behaviors (Mishra and Hoon, 2013; Sun and Chen, 2007; Sun et al., 2009; Wan et al., 2017); and (3) genetic ablation of vesicular glutamate transporter subtype 2 (*Vglut2*) in primary nociceptors and itch-sensing afferents leads to decreased pain but increased itch behaviors (Lagerström et al., 2010, 2011; Liu et al., 2010; Ma, 2014; Rogoz et al., 2012; Scherrer et al., 2010). Because *Vglut2* is the main vesicular glutamate transporter gene expressed in these neurons, these results suggest that glutamate is required for nociception but dispensable for itch transmission (Ma, 2014). It is worth noting, however, that no physiological recordings have directly confirmed that glutamate transmission is disrupted in the primary itch-sensing afferents of *Vglut2* conditional knockout (CKO) mice.

Surprisingly, the neurotransmitters used by MRGPRA3$^+$ primary afferents remain unclear. Several groups found that the expression of *Grp* transcripts in normal mouse DRG and TG neurons is almost undetectable, as shown by *in situ* hybridization, RT-PCR, and RNA sequencing (Fleming et al., 2012; Goswami et al., 2014; Li et al., 2018; Mishra et al., 2012; Nguyen et al., 2017; Usoskin et al., 2015). The GRP antibody used to show its expression in mouse DRG neurons displays cross reactivity to substance P (Solorzano et al., 2015). Instead, *Grp* is highly expressed in a population of spinal cord DH interneurons that function in itch-sensing pathways (Albisetti et al., 2019; Fleming et al., 2012; Kiguchi et al., 2020; Mishra and Hoon, 2013; Pagani et al., 2019) and may serve as a "leaky gate" for nociceptive signals (Sun et al., 2017). In addition, *Nppb* is expressed in primary sensory neurons distinct from MRGPRA3$^+$ afferents (Solinski et al., 2019; Usoskin et al., 2015). To fill this knowledge gap and test the ''itch-selective neurotransmitter'' model, we sought to investigate the functions of candidate neurotransmitters in MRGPRA3$^+$ primary afferents in synaptic transmission and itch behaviors.

Here, we found that glutamate is an essential neurotransmitter in MRGPRA3$^+$ afferents for mediating synaptic transmission and acute/chronic itch behaviors. Moreover, the neuropeptide neuromedin B (*Nmb*) is highly expressed in MRGPRA3$^+$ neurons, which form monosynaptic, glutamatergic connections with NMBR$^+$ and NMBR$^-$ DH neurons and function in a context-dependent manner (pruritogen type, concentration, etc.) to enhance the activity of NMBR$^+$ DH neurons. These findings shed new light on the neurotransmitters used by MRGPRA3$^+$ afferents for itch transmission. Given the general use of glutamate in sensory neurons and the broad expression pattern of *Nmb* in itch-sensing and nociceptive primary afferents, our data argue that activation of specific combinations of postsynaptic neurons, rather than utilization of modality-selective neurotransmitters, may underlie itch specificity.

RESULTS

Optogenetic activation of MRGPRA3$^+$ primary afferents triggers itch-related behaviors

To specifically activate itch-selective MRGPRA3$^+$ primary afferents, we crossed *Mrgpra3^{Cre}* transgenic mice with conditional *ChR2* (*Rosa$^{ChR2\text{-}EYFPf/f}$*, *Ai32*) mice to generate *Mrgpra3-ChR2* (*Mrgpra3^{Cre}*; *Rosa$^{ChR2\text{-}EYFPf/f}$*) mice (Figure 1A), in which ChR2 would be specifically expressed in MRGPRA3-Cre$^+$ neurons. We used homozygous Ai32 alleles because mice with heterozygous alleles showed minimal behavioral responses in our pilot experiments. To confirm expression of ChR2 in MRGPRA3$^+$ neurons, we performed double fluorescent RNAscope *in situ* hybridization on DRG sections using probes against *Mrgpra3* and *EYFP* (specific to the *ChR2-EYFP* fusion transcript) and found that all *Mrgpra3*$^+$ neurons were *EYFP*$^+$, whereas most (82%) of the *EYFP*$^+$ neurons were also *Mrgpra3*$^+$ (Figure S1H). Double immunostaining using antibodies against GFP (recognizing both nucleus-localized *Mrgpra3$^{Cre\text{-}EGFP}$* and membrane-localized ChR2-EYFP fusion protein) and other primary afferent neuronal markers showed that 13.0% and 38.7% of membrane GFP$^+$ neurons overlap with CGRP (a marker for peptidergic nociceptors) and IB4 (a marker for non-peptidergic nociceptors), respectively, but showed almost no overlap with NF200 (a marker for large diameter mechanoreceptors, 0.5%) in lumbar DRG sections (Figures S1A–S1C). The central terminals of GFP$^+$ afferents innervate superficial layers (layer II) of the spinal DH (Figures S1D–S1F). Together, our histological data validate the specific expression of ChR2 in MRGPRA3$^+$ primary afferents.

Using high-speed imaging, we recorded behavioral responses to peripheral blue laser stimulation of the de-haired cheek and nape of 2- or 6-month-old freely behaving *Mrgpra3-ChR2* and control (*Ai32*) mice. During and within the first few seconds of a brief blue light stimulus, *Mrgpra3-ChR2* but not control mice. displayed scratching (S), ipsilateral hind paw lifting (indicating urge to scratch) (PL), head shaking (HS), and asymmetric/symmetric bilateral forepaw wiping (BW) in a laser-intensity-dependent manner (Figures 1B, 1C, and S2M–S2O; Table S1; Videos S1 and S2). We found little ipsilateral unilateral forepaw wiping behavior (UW), in which the contralateral forepaw was touching the ground. In short, our optical activation of MRGPRA3$^+$ afferents induced scratching and related avoidance behaviors, similar to previous publications (Sharif et al., 2020; Sun et al.,

(D–J) Double fluorescent *in situ* hybridization of *Mrgpra3* (green) and *Nmb, Tac1, Nppb, Calca*, and vesicular glutamate transporters *Vglut1, Vglut2*, and *Vglut3* (red) using lumbar DRG sections of 3-week-old wild-type mice. Arrowheads indicate some *Mrgpra3*$^+$ neurons. Pie charts show the quantification. Scale bars, 50 μm. 6–8 sections/mouse, n = 3.

(K) Schematic of recording from superficial DH neurons using spinal cord slices of 4 - to 6-week-old *Mrgpra3-ChR2* mice.

(L and M) Representative traces of repetitive blue laser-induced EPSCs (EPSC $_L$s). Monosynaptic or polysynaptic EPSC$_L$s were differentiated by 0.2 Hz, 20 times blue laser stimuli (blue arrows). Quantification of monosynaptic, polysynaptic, and non-response types is shown in the table.

(N–Q) In neurons with light stimulation-induced monosynaptic responses (N), monosynaptic EPSC $_L$s (O, black trace), EPSP$_L$s (P, black trace), and action potentials (Q, black trace) were completely blocked by glutamate receptor antagonists, NBQX (20 μM) and AP5 (50 μM) (red traces). Data are presented as mean ± SEM. See also Figures S1 and S2, Table S1, and Videos S1 and S2

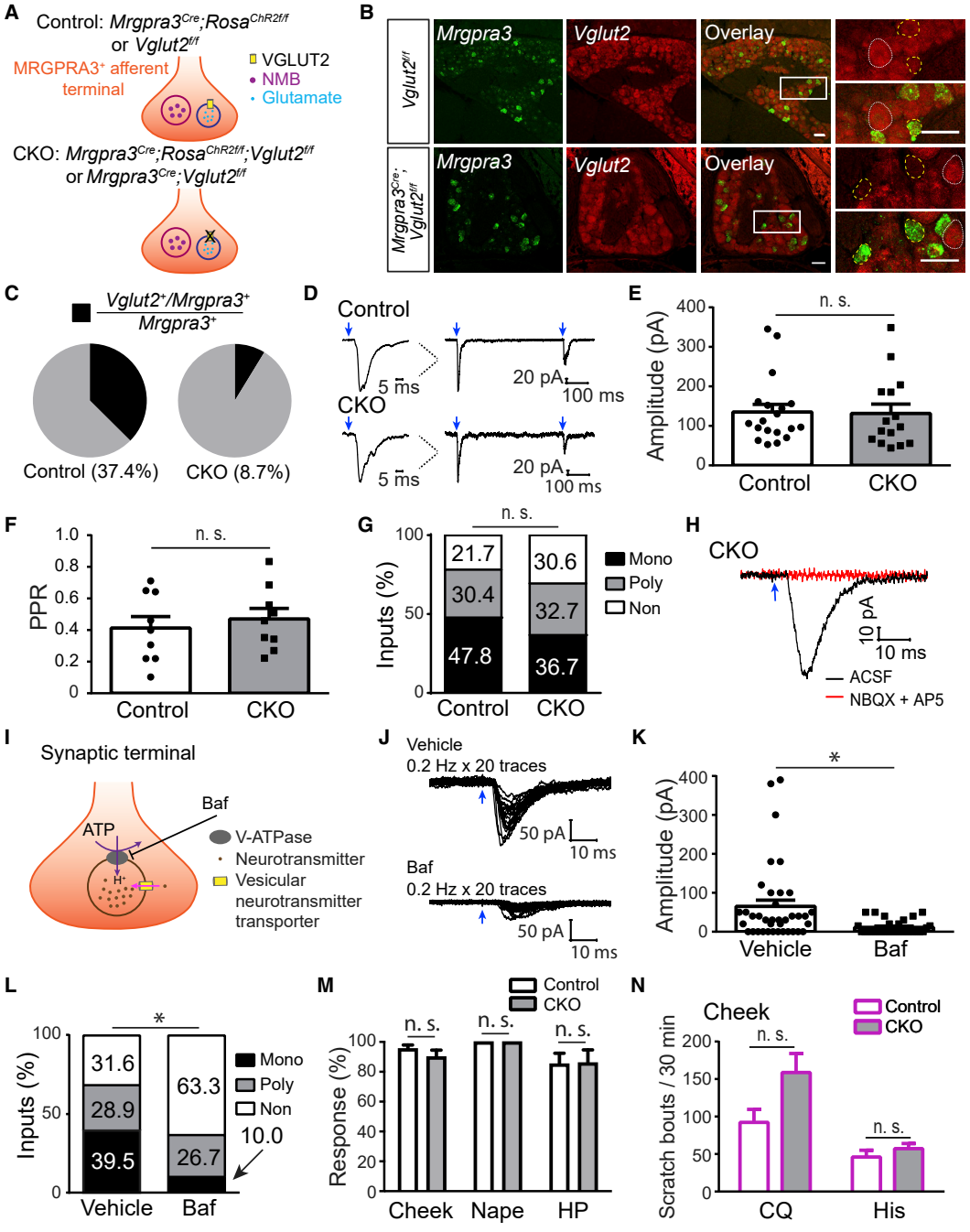

Figure 2. Light-induced synaptic responses and behaviors are retained in juvenile and young adult *Mrgpra3-Vglut2* CKO mice

(A) Illustration showing MRGPRA3$^+$ afferent terminal of *Mrgpra3*^{Cre}; *Rosa*$^{ChR2f/f}$ (control) and *Mrgpra3*^{Cre}; *Rosa*$^{ChR2f/f}$; *Vglut2*$^{f/f}$ (*Mrgpra3-Vglut2* CKO) mice.

(B) Double fluorescent *in situ* hybridization of *Mrgpra3* (green) and *Vglut2* (red) in DRG sections of *Vglut2*$^{f/f}$ and CKO mice at 3 weeks of age. Images in the rectangles are enlarged. White circles indicate *Vglut2*$^+$*Mrgpra3*$^-$ neurons. Yellow circles indicate *Mrgpra3*$^+$ neurons. Scale bars, 50 μm. 6–8 sections/mouse, n = 3.

(C) Quantification of *Vglut2*$^+$*Mrgpra3*$^+$ cells in lumbar and thoracic DRG of 3-week-old control and CKO mice. 1–6 sections/mouse, n = 2–3.

(D) Representative paired light stimulation-induced monosynaptic EPSC traces recorded from superficial DH neurons of 4- to 6-week-old control and CKO mouse spinal cord slices.

(E and F) Quantification of monosynaptic $EPSC_L$ amplitude and PPR in control and CKO groups.

(G) Quantification of response-type proportion in control and CKO mice.

(legend continued on next page)

2017). Because optogenetic stimulation can evoke scratching, an itch-specific behavior, some circuits triggered by light stimulation of MRGPRA3$^+$ afferents must contribute to itch transmission.

Mrgpra3$^+$ primary afferents highly express *Nmb* and *Vglut2*

To identify the neurotransmitter(s) released from MRGPRA3$^+$ primary afferents, we first performed a bioinformatics analysis using published RNA-seq data of DRG and TG neurons (Chiu et al., 2014; Li et al., 2016; Usoskin et al., 2015) and found that *Nmb* and *Vglut2* are highly expressed in *Mrgpra3*$^+$ afferents. To confirm this finding, we performed double fluorescent *in situ* hybridization of DRG neurons using probes against *Mrgpra3*, *Vglut1-3*, and neuropeptides (*Nmb, Tac1, Nppb*, and *Calca*) previously shown to be expressed in primary afferents. *Nmb* is highly expressed in almost all *Mrgpra3*$^+$ neurons, whereas little overlap is found between *Mrgpra3* and *Tac1* or *Nppb*. 14.4% of *Mrgpra3*$^+$ neurons expressed *Calca* (Figures 1D–1G). Consistent with previous publications (Fleming et al., 2012; Li et al., 2018; Mishra and Hoon, 2013; Solorzano et al., 2015), we were unable to detect *Grp* transcripts in wild-type DRG neurons using RNAscope *in situ* hybridization (Figure S1G) (as a positive control, this probe detected positive spinal cord DH neurons, Figure S6L). In addition, we found that 89.6% of *Mrgpra3*$^+$ neurons are *Vglut2*$^+$, whereas *Vglut1* and *Vglut3* were barely detected in *Mrgpra3*$^+$ neurons (Figures 1H–1J). Together, our results suggest that glutamate and/or NMB might be candidate neurotransmitters used by MRGPRA3$^+$ primary afferents for itch transmission.

MRGPRA3$^+$ primary afferents communicate with spinal DH neurons through glutamate

To examine the synaptic transmission between MRGPRA3$^+$ primary afferents and postsynaptic DH neurons, we performed spinal cord slice recordings with 4- to 6-week-old *Mrgpra3-ChR2* mice (Figure 1K). In whole cell patch clamp recordings from layer II DH neurons located in the ChR2$^+$ afferent-innervating territory, mono- or polysynaptic responses were differentiated based on the jitter and failure rate of the responses to 0.2 Hz, 20 pulses of blue laser stimuli (Cui et al., 2016; Wang and Zylka, 2009). Around 48% and 30% of recorded neurons showed predominantly mono- and polysynaptic light-evoked excitatory postsynaptic currents ($EPSC_{LS}$), respectively, whereas 22% of recorded neurons did not show a response (Figures 1L and 1M, 46 neurons total). To further validate our classification of mono- or polysynaptic transmission, light-evoked responses were first recorded in artificial cerebrospinal fluid (ACSF) and then in the presence of the sodium channel blocker tetrodotoxin toxin (TTX, 1 μM), followed by TTX with 4-aminopyridine (4-AP, 4 mM) (Wallace et al., 2017). For neurons displaying monosynaptic connectivity, their $EPSC_L$s were completely blocked by TTX but recovered by TTX and 4-AP treatment (Figures S2A–S2D). In contrast, for neurons displaying polysynaptic responses, their $EPSC_L$s were completely blocked by TTX and were not recovered by TTX and 4-AP treatment (Figures S2E–S2H). Moreover, we removed the cytosol of a few monosynaptic postsynaptic neurons and performed single-cell RT-PCR of *Gapdh*, *Grp*, *Grpr*, and *Nmbr* (Figures S2K–S2L). A small percentage of these neurons were GRP$^+$ or NMBR$^+$, but none were GRPR$^+$. To test for glutamate release from MRGPRA3$^+$ afferents, we applied glutamate receptor antagonists NBQX (20 μM) and AP5 (50 μM) and found that monosynaptic $EPSC_L$s were completely blocked by glutamate receptor antagonists (Figures 1N and 1O). Because secondary messengers critical for GPCR signaling may be diluted or lost in the whole cell configuration, we also conducted similar experiments using perforated patch clamp recordings with amphotericin B (100 μg/ml) and found similar results (Figure S2I). Light also evoked EPSPs and action potentials (4/11 neurons) in some monosynaptic downstream neurons, which were completely blocked by glutamate receptor antagonists (Figures 1P, 1Q, and S2J). Taken together, our data indicate that MRGPRA3$^+$ primary afferents mainly release glutamate for synaptic transmission upon optical stimulation and form monosynaptic connections with GRP$^+$, NMBR$^+$, and other types of DH neurons.

Glutamatergic transmission and somatosensory behaviors are normal in juvenile and young adult *Mrgpra3-Vglut2* CKO mice

To determine the role of glutamate release from MRGPRA3$^+$ primary afferents in itch transmission, we generated *Mrgpra3-Vglut2* CKO (*Mrgpra3*^{Cre}; *Vglut2*$^{f/f}$ *or Mrgpra3*^{Cre}; *Vglut2*$^{f/f}$; *Rosa*$^{ChR2f/f}$) and control (*Vglut2*$^{f/f}$ or *Mrgpra3*^{Cre}; *Rosa*$^{ChR2f/f}$) mice (Figures 2A and S3A). We confirmed the cell-type-specific knockout of *Vglut2* using single-cell RT-PCR with dissociated *Mrgpra3*$^+$ DRG neurons and double fluorescent *in situ* hybridization (Figures S3B, S3C, 2B, and 2C). We found that there was no upregulation of *Vglut1* and *Vglut3* in *Mrgpra3*$^+$ DRG neurons to compensate for the loss of *Vglut2* (Figures S3C–S3G).

Next, we examined synaptic transmission from MRGPRA3$^+$ primary afferents by recording $EPSC_L$s from DH neurons using spinal cord slices of 4- to 6-week-old control and *Mrgpra3-Vglut2* CKO mice. Because most *Mrgpra3*$^+$ primary afferents

(H) A representative trace of a monosynaptic $EPSC_L$ (black trace) recorded from a superficial DH neuron in a CKO mouse spinal cord slice, which is completely blocked by glutamate receptor antagonists, NBQX and AP5 (red trace).
(I) Diagram showing effect of bafilomycin A1 (Baf) on synaptic transmission.(J) Representative traces of monosynaptic $EPSC_L$s recorded from superficial DH neurons of CKO mouse spinal cord slices after vehicle or bafilomycin A1 treatments.
(K and L) Quantification of $EPSC_L$ amplitude and response-type proportion in bafilomycin A1- or vehicle-treated groups in CKO mice.
(M) The percentage of responses induced by light stimulation of the cheek, nape, or hind paw (HP) was not significantly different between control and CKO mice around 2 months of age.
(N) CQ- or histamine-induced scratch bouts after cheek injections were not significantly different between control and CKO mice. Data are presented as mean ± SEM. Unpaired Student's t test in (E, F, K, M, and N); chi-square test in (G and L). *$p < 0.05$; n.s., not significant. See also Figures S3 and S4, Table S2, and Video S3

express *Vglut2* but not *Vglut1* and *Vglut3* (Figures 1H–1J), we hypothesized that *Mrgpra3-Vglut2* CKO neurons would exhibit decreased glutamate transmission. Surprisingly, the amplitude (control 135.2 ± 19.2 pA, n = 19; CKO 131.6 ± 23.4 pA, n = 15, $p > 0.05$) and paired pulse ratio (PPR; control 0.41 ± 0.07, n = 9; CKO 0.47 ± 0.07, n = 9, $p > 0.05$) of monosynaptic $EPSC_L$s recorded from CKO mice did not show any obvious reduction compared with control mice (Figures 2D–2F). There was also no significant difference in light-induced proportions of $EPSC_L$ response types (monosynaptic, polysynaptic, or non-responses) between control and *Mrgpra3-Vglut2* CKO mice (Figure 2G). Furthermore, the $EPSC_L$s of CKO mice were completely abolished by glutamate antagonists NBQX (20 μM) and AP5 (50 μM) (Figure 2H). Together, our results indicate that there is no obvious deficit in glutamatergic transmission from *Vglut2*-null MRGPRA3$^+$ primary afferents at 4 to 6 weeks of age.

To determine whether glutamate release from MRGPRA3$^+$ primary afferents in *Mrgpra3-Vglut2* CKO mice at this age is still vesicle-dependent, we recorded from spinal cord slices pretreated with bafilomycin A1 (4 mM). Bafilomycin A1 affects vesicle-dependent neurotransmitter release by inhibiting vesicular ATPase and thus reduces the electrochemical gradient of H^+ in vesicles (Figure 2I) (Dröse and Altendorf, 1997). Bafilomycin A1 treatment greatly reduced the amplitude of $EPSC_L$s (vehicle 65.0 ± 16.0 pA, n = 38; bafilomycin A1 11.3 ± 3.2 pA, n = 30, unpaired t test $p < 0.05$) and the overall percentage of responsive neurons of *Mrgpra3-Vglut2* CKO mice compared with vehicle control (Figures 2J–2L). In addition, bafilomycin A1 attenuated the frequency (vehicle 8.4 ± 1.3 Hz, n = 37 versus bafilomycin A1 2.4 ± 0.7 Hz, n = 30, $p < 0.05$) but not the amplitude (vehicle 24.3 ± 0.6 pA, n = 37 versus bafilomycin A1 22.5 ± 0.7 pA, n = 30, $p > 0.05$) of sEPSCs (Figures S4A–S4C). These results suggest that 4- to 6-week-old *Vglut2*-knockout *Mrgpra3*$^+$ primary afferents still release glutamate in a vesicle-dependent manner.

Consistent with the almost intact synaptic transmission in juvenile *Mrgpra3-Vglut2* CKO mice, mutant mice around 2 months old display normal cheek and nape scratching and avoidance behaviors in response to optical stimulation (cheek: control 95.5% ± 2.5% versus CKO 90.0% ± 4.5%, $p > 0.05$; nape: control 100.0% ± 0% versus CKO 100.0% ± 0%, $p > 0.05$, control n = 11, CKO n = 5) (Figure 2M). Hind paw optical stimulation responses, including hind paw shaking or lifting, were also unaffected (control 85.2% ± 7.2% versus CKO 86.0 ± 8.7, $p > 0.05$, Video S3). In addition, pruritogen (CQ, histamine, SLIGRL, BAM8-22, and 5-HT) cheek and nape injection-induced scratching responses were similar between *Mrgpra3-Vglut2* CKO and control mice (Table S2; Figures 2N, S4D, and S4E). These mice also displayed similar spontaneous scratching (cheek: control 8.2 ± 1.9 bouts/30 min versus CKO 9.3 ± 1.8 bouts/30 min $p > 0.05$; nape: control 2.0 ± 0.7 bouts/30 min; CKO 2.5 ± 0.9 bouts/30 min, $p > 0.05$. n = 10 for control and n = 8 for CKO) behaviors. No deficits were found in mechanosensitivity or thermal pain-related behavior assays compared with control mice (Figures S4F–S4J). Collectively, our results reveal that glutamatergic transmission as well as itch-related and other somatosensory behaviors are retained in juvenile/young adult *Mrgpra3-Vglut2* CKO mice.

Loss of glutamate transmission is age-dependent in *Trpv1-Vglut2* CKO mice

Given that the same *Vglut2* conditional allele has been widely used to mitigate glutamate release and examine glutamate function in the nervous system (Liu et al., 2010; Roccaro-Waldmeyer et al., 2018; Tong et al., 2007), we were puzzled by the lack of reduction in glutamate transmission in young *Mrgpra3-Vglut2* CKO mice. Because *Vglut2* CKO in nociceptors was reported to show reduced pain but increased itch sensitivity (Lagerström et al., 2011; Lagerström et al., 2010; Liu et al., 2010; Ma, 2014; Rogoz et al., 2012; Scherrer et al., 2010), we generated nociceptor-specific *Trpv1-Vglut2* CKO (*Trpv1*^{Cre}; *Rosa*$^{ChR2f/f}$; *Vglut2*$^{f/f}$) and control (*Trpv1*^{Cre}; *Rosa*$^{ChR2f/f}$) mice to examine their synaptic transmission and spontaneous itch behaviors at different ages (Figure 3A). Using spinal cord slices of 4- to 5-week-old control and CKO mice, we found that neither the $EPSC_L$s amplitude (control 634.4 ± 162.2 pA, n = 16 versus CKO 507.5 ± 165.9 pA, n = 8, $p > 0.05$) nor response-type proportions (for both cohorts, 100% of responsive cells exhibited monosynaptic type responses) showed a significant difference between control and *Trpv1-Vglut2* CKO mice (Figures 3B and 3C). *Trpv1-Vglut2* CKO mice at this age also did not show increased itch sensitivity (spontaneous scratching). Thus, similar to juvenile *Mrgpra3-Vglut2* CKO mice, *Trpv1-Vglut2* CKO mice that are 5 weeks old or younger show no deficit in glutamate transmission and itch behaviors.

Interestingly, we observed that *Trpv1-Vglut2* CKO mice showed increased spontaneous scratching when they were around 6 weeks old. This phenotype became dramatic around 8 weeks of age (control 5.3 ± 2.9 bouts/30 min, n = 3 versus CKO 264.8 ± 75.4 bouts/30 min, n = 5, $p < 0.05$) (Figure 3D) when the CKO mice developed skin lesions. In recordings from spinal cord slices of 8-week-old control and *Trpv1-Vglut2* CKO mice, we found significant reductions in $EPSC_L$ amplitude (control 588.3 ± 118.5 pA, n = 16 versus CKO 271.4 ± 60.6 pA, n = 30, $p < 0.05$) and response-type proportion (control: monosynaptic 100% versus CKO: monosynaptic 76.7%, polysynaptic 20%, non-responsive 3.3%) in CKO mice compared with control mice (Figures 3E and 3F). Our results reveal an age-dependent loss of glutamate transmission in *TrpV1-Vglut2* CKO primary afferents.

Loss of glutamate transmission and reduction of itch behaviors occurs in 6-month-old *Mrgpra3-Vglut2* CKO mice

Given that *Mrgpra3-Vglut2* CKO afferents still retain glutamate transmission up to 2 months of age (Figures 2D–2H), it is possible that the age when glutamate transmission is eliminated varies in different *Vglut2* CKO mice. To identify the age at which *Mrgpra3-Vglut2* mice lose glutamate transmission, we performed peripheral optogenetic stimulation of 4- and 6-month-old *Mrgpra3-Vglut2* mice and used their responses as a proxy. We found that only 6-month-old *Mrgpra3-Vglut2* CKO mice greatly reduced their responsiveness to peripheral blue laser stimuli (cheek: control 97.5 ± 1.6% versus CKO 16.0% ± 6.5%, $p <$ 0.05; the nape of the neck: control 100.0% ± 0%, versus CKO 6.0% ± 4.3%, %, $p < 0.05$; hind paw: control 78.8% ± 7.4% versus 24.0% ± 5.9%, $p < 0.05$; control n = 8, CKO n = 10) (Figure 4O; Video S4). Histological examination of DRG, spinal cord,

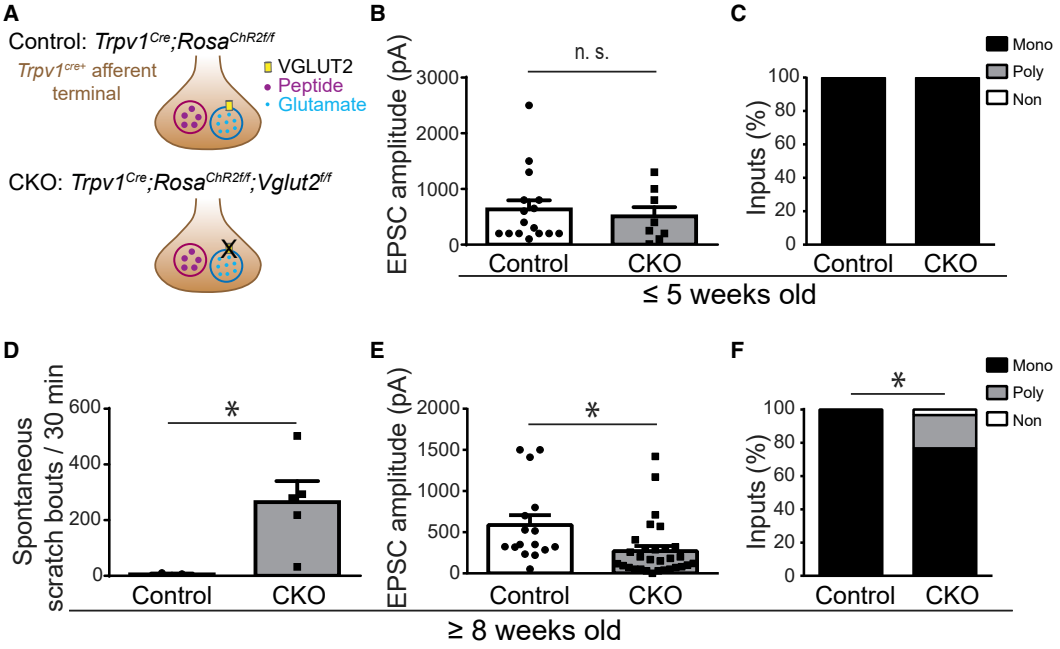

Figure 3. Age-dependent deficits in synaptic transmission and itch behaviors of *Trpv1-Vglut2* CKO mice

(A) Illustration showing afferent terminals of *Trpv1*^{Cre}; *Rosa*$^{ChR2f/f}$ (control) and *Trpv1*^{Cre}; *Rosa*$^{ChR2f/f}$; *Vglut2*$^{f/f}$ (*Trpv1-Vglut2* CKO) mice.

(B and C) Quantification of amplitude of EPSC$_L$s and input proportion of recorded superficial DH neurons in spinal cord slices of ≤5-week-old control and CKO mice.

(D) Quantification of spontaneous scratching in ≥8-week-old control and CKO mice.

(E and F) Quantification of amplitude of EPSC$_L$s and response-type proportion of recorded superficial DH neurons in spinal cord slices in ≥8-week-old control and CKO mice. Data are presented as mean ± SEM. Unpaired Student's t test in (B, D, and E); chi-square test in (C and F). *p < 0.05; n.s., not significant.

and hairy skin sections of 6-month-old control and CKO mice revealed no gross anatomical differences (Figures 4A–4J). The cell count (control 34.1 ± 2.2 neurons/section versus CKO 28.3 ± 5.9 neurons/section, p > 0.05) and expression of molecular markers of ChR2$^+$ DRG neurons (IB4$^+$ChR2$^+$/ChR2$^+$: control 67.7% ± 2.4% versus CKO 69.0% ± 1.7%, p > 0.05; CGRP$^+$ChR2$^+$/ChR2$^+$: control 33.1% ± 8.1% versus CKO 39.2% ± 11.9%, p > 0.05; NF200$^+$ChR2$^+$/ChR2$^+$: control 3.3% ± 0.9% versus CKO 3.7% ± 0.8%, p > 0.05) were also comparable (Figures 4K and 4L) suggest that *Vglut2* ablation in MRGPRA3$^+$ afferents does not cause obvious anatomical or molecular marker changes.

To confirm the loss of glutamate release, we examined synaptic transmission by recording EPSC$_L$s from DH neurons of 6-month-old control and *Mrgpra3-Vglut2* CKO mice. Indeed, the amplitudes of EPSC$_L$s were significantly reduced in CKO compared with control mice (control 192.9 ± 27.5 pA, n = 40 versus CKO 24.2 ± 7.8 pA, n = 31, p < 0.05) (Figure 4M), and a much higher proportion of DH neurons recorded from CKO mice showed no responses (control: monosynaptic 85.0%, polysynaptic 15.0%, non-responsive 0% versus CKO: monosynaptic 6.4%, polysynaptic 32.3%, non-responsive 61.3%) (Figure 4N). Therefore, using *Mrgpra3-Vglut2* mice that are 6 months old or older would allow us to determine the contribution of glutamate to itch transmission. Indeed, CKO mice showed attenuated scratching elicited by pruritogen injections, such as CQ or histamine (CQ: control 60.0 ± 7.7 bouts/30 min, n = 12 versus CKO 30.3 ± 8.0 bouts/30 min, n = 14, p < 0.05; histamine: control 35.9 ± 9.1 bouts/30 min, n = 8 versus CKO 11.9 ± 1.9 bouts/30 min, n = 9, p < 0.05) (Figure 4P). These mice showed no deficits in mechanical sensitivity (Figures S5A–S5E). Moreover, we tested control and CKO mice with a mouse model of contact dermatitis by treating with topical squaric acid dibutyl ester (SADBE) (Qu et al., 2014), which induced parakeratosis (Figures S5F and S5G) and spontaneous scratching. Spontaneous itch was greatly reduced in CKO mice compared with control mice (control 45.8 ± 14.3 spontaneous scratching bouts/30 min, n = 5 versus CKO 11.9 ± 5.3 bouts/30 min, n = 7, p < 0.05) (Figure 4Q). Taken together, our results demonstrate that glutamate transmission is not lost in *Mrgpra3-Vglut2* primary afferents until these mice are at least 6 months old. Because both chemical-induced acute itch and chronic spontaneous itch behaviors are greatly reduced when glutamate transmission is eliminated in these mutant mice, our results indicate that glutamate plays an essential role in synaptic transmission for primary itch-sensing afferents and in itch behaviors.

Characterization of NMBR$^+$ DH neurons

To investigate the role of NMB in itch transmission, we generated an *Nmbr*^{Cre} knockin mouse line (Figure 5A) and specifically

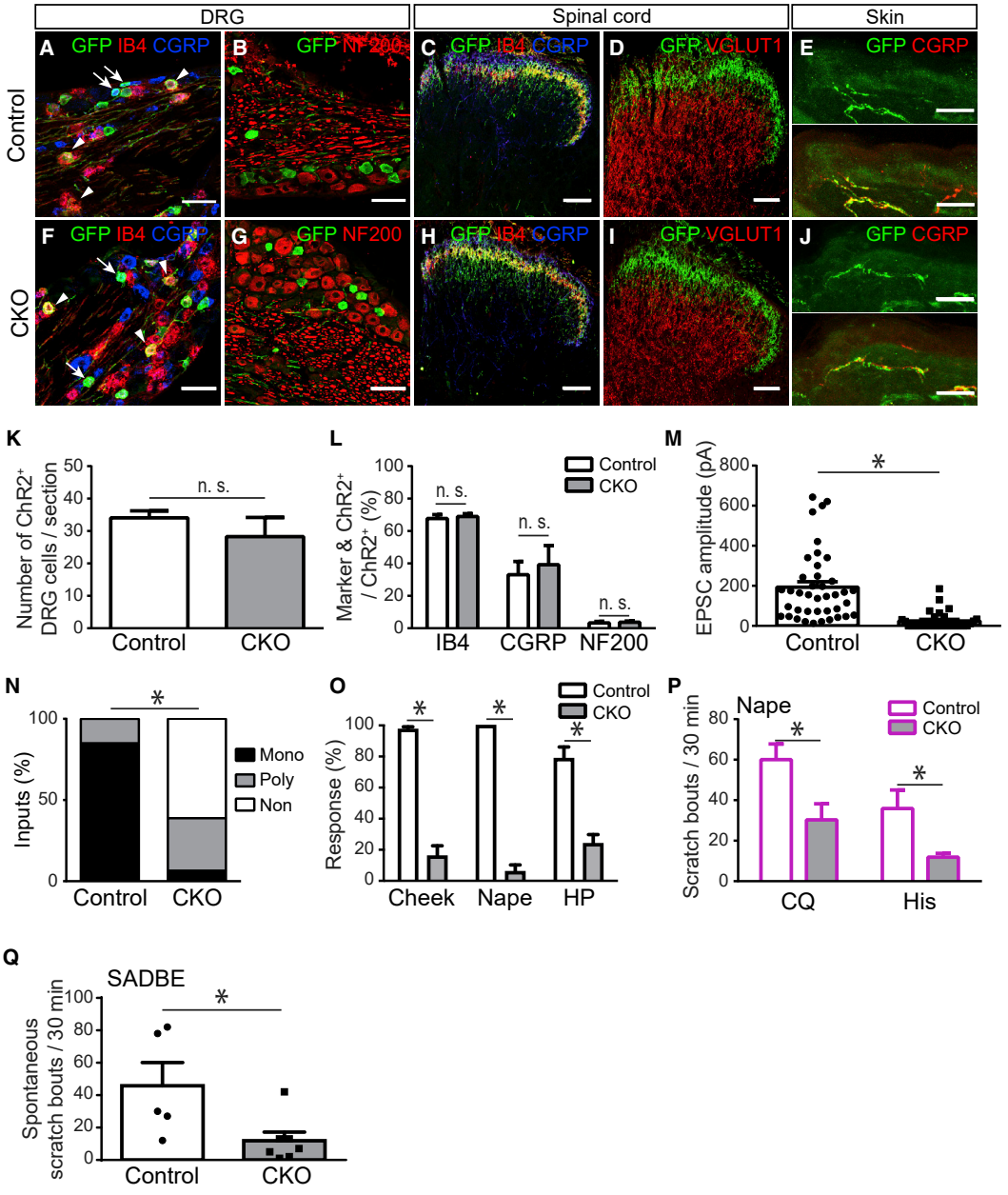

Figure 4. *Mrgpra3-Vglut2* CKO mice display deficits in synaptic transmission and itch behaviors at 6 months and older

(A–J) Immunostaining of molecular markers with sections from lumbar (L4 and L5) DRG, lumbar spinal cord, and hairy skin of ≥6-month-old control and *Mrgpra3-Vglut2* CKO mice. Scale bars: DRG 50 μm, spinal cord 50 μm, skin 10 μm.

(K and L) Quantification of number of ChR2$^+$ neurons in DRG sections and percentage of ChR2$^+$ neurons expressing different molecular markers. 6–8 sections/mouse, n = 3.

(M and N) Quantification of amplitude of EPSC$_L$s and response-type proportions of recorded superficial DH neurons in spinal cord slices of ≥6-month-old control and CKO mice.

(O) Quantification of the responses induced by cheek, nape, or hind paw (HP) light stimulation in control and CKO mice.

(P) Quantification of scratch bouts in response to the nape of the neck injections of CQ or histamine in control and CKO mice.

(Q) Quantification of SADBE-induced spontaneous scratch bouts in control and CKO mice. Data are presented as mean ± SEM. Unpaired Student's t test in (K, L, M, O, P, and Q); chi-square test in (N). *p < 0.05; n.s., not significant. See also Figure S5 and Video 4

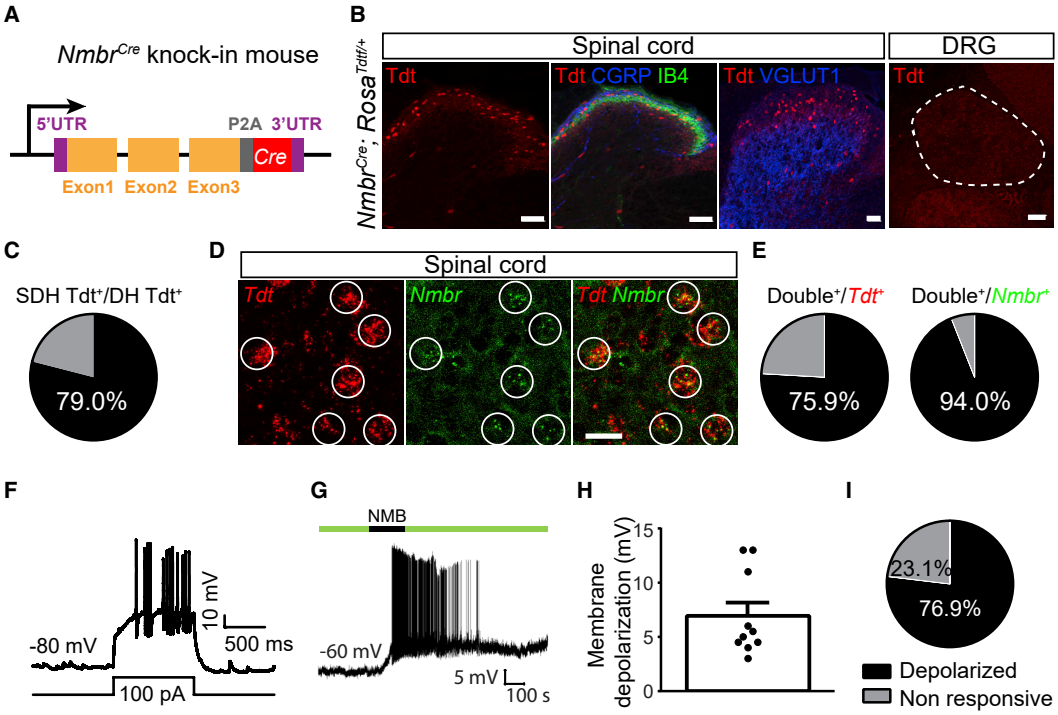

Figure 5. NMB depolarizes the membrane potential of NMBR$^+$ spinal DH neurons

(A) Diagram showing genomic structure of *Nmbr^{cre}* knockin mouse line.

(B) Co-staining of Tdt and molecular markers with lumbar spinal cord and DRG (L4 and L5) sections from 3-week-old *Nmbr-Tdt* mice. There is no Tdt expression in DRG neurons. Scale bars: 50 μm.

(C) Quantification of Tdt$^+$ cell distribution in the spinal cord DH, 6–8 sections/mouse, n = 3.

(D) RNAscope *in situ* hybridization of *Tdt* and *Nmbr* with lumbar spinal DH sections of 3-week-old *Nmbr-Tdt* mice. Scale bars: 10 μm.

(E) Quantification of double-positive cells among *Tdt*$^+$ cells or *Nmbr*$^+$ cells in the spinal cord DH superficial layers. 6–8 sections/mouse, n = 3.

(F) A representative firing pattern trace of Tdt$^+$ cells in response to rectangular current injection in current clamp mode with spinal cord slices of 5- to 6-week-old *Nmbr-Tdt* mice. All recorded Tdt$^+$ neurons showed a delayed firing pattern.

(G) A representative trace of NMB (2 μM) perfusion-induced membrane depolarization and action potential firing in Tdt$^+$ cells using perforated patch clamp recording with pretreatment of ionotropic receptor antagonists.

(H and I) Quantification of NMB perfusion-induced membrane depolarization and the percentage of Tdt$^+$ cells responsive to NMB application (n = 13 neurons). Each dot indicates one responsive Tdt$^+$ neuron. Data are presented as mean ± SEM. See also Figure S6.

labeled cells expressing the NMB receptor (NMBR) by crossing *Nmbr^{Cre}* with a Cre-dependent Tdtomato reporter line (*Rosa$^{Tdtf/f}$*, Ai9). Tdt$^+$ neurons are found in the spinal cord DH but not in DRGs (Figures 5B and 5C), and most Tdt$^+$ cells (79%) are located in the DH superficial layer. RNAscope *in situ* hybridization for *Tdt* and spinal cord neuronal markers revealed that 75.9% of *Tdt*$^+$ cells are *Nmbr*$^+$, whereas *Tdt*$^+$ cells make up 94% of *Nmbr*$^+$ cells in the superficial DH (Figures 5D and 5E). In addition, 81.4% of *Tdt*$^+$ cells are *Vglut2*$^+$, 86.0% are *Tac1*$^+$, and 63.1% are *Sst*$^+$, whereas only a small percentage of *Tdt*$^+$ cells co-express *Vgat* (14.9%), *Grp* (19.5%), *Grpr* (13.0%), *Npr1* (13.3%), or *Tacr1* (5.5%) in the superficial DH (Figure S6). Our results suggest that recombination in this *Nmbr^{Cre}* knockin mouse line largely recapitulates the expression of endogenous *Nmbr* and that most *Nmbr*$^+$ superficial DH cells are Tac1$^+$/SST$^+$ excitatory interneurons, which correlate with the Glut10-11 DH neurons defined by transcriptome profiling analysis (Häring et al., 2018). Consistently, all recorded Tdt$^+$ neurons exhibited a delayed firing pattern (Figure 5F), a characteristic of excitatory interneurons (Yasaka et al., 2010). To examine functional NMB receptor expression in Tdt$^+$ cells, we perfused NMB while performing perforated patch clamp recordings from Tdt$^+$ cells in spinal cord slices pretreated with ionotropic receptor antagonists (20 μM NBQX, 50 μM AP5, 10 μM bicuculline, and 0.4 μM strychnine). NMB perfusion depolarized membrane potentials (7.0 ± 1.2 mV, n = 10), resulting in action potential firing in 76.9% of the recorded Tdt$^+$ cells (Figures 5G–5I). Together, our results suggest that functional NMB receptors are expressed in *Nmbr-Tdt* excitatory interneurons and that NMB alone can depolarize these neurons and trigger action potentials.

MRGPRA3$^+$ primary afferents directly synapse with NMBR$^+$ DH neurons

We reasoned that if NMB functions as a neurotransmitter in MRGPRA3$^+$ afferents, MRGPRA3$^+$ afferents may form monosynaptic connections with NMBR$^+$ DH neurons, as suggested

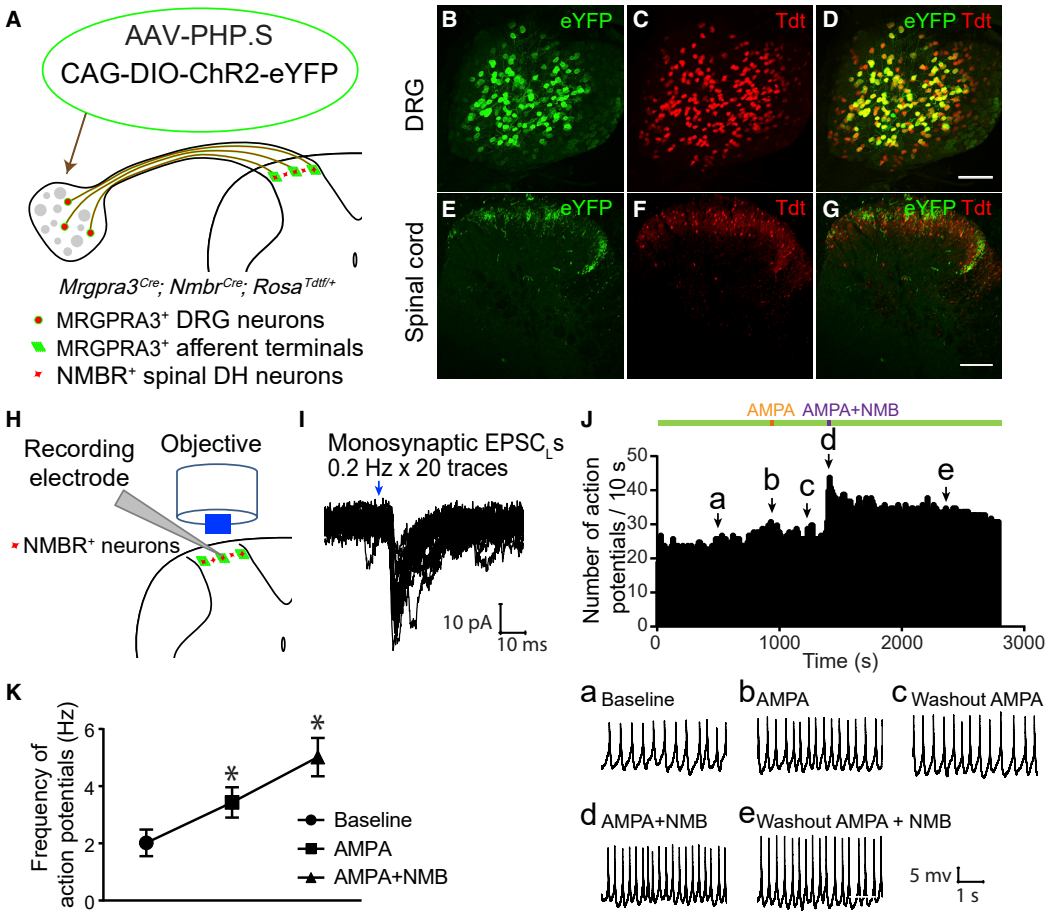

Figure 6. NMBR$^+$ DH neurons receive monosynaptic inputs from MRGPRA3$^+$ primary afferents and NMB enhances the activity of NMBR$^+$ DH neurons through synergy with glutamate

(A) Diagram showing the genetic and viral strategies to specifically express ChR2 in MRGPRA3$^+$ afferents and genetically label NMBR$^+$ DH neurons with Tdt.

(B–G) Expression of ChR2 and Tdt in a whole mount lumbar DRG (B–D) and spinal cord sections (E–G). Scale bars: 100 μm.

(H) Diagram showing targeted recordings of *Nmbr-Tdt* DH neurons while specifically stimulating MRGPRA3$^+$ primary afferents with blue laser.

(I) Representative traces of light-induced monosynaptic EPSC $_L$s in response to 0.2 Hz, 20 times stimuli.

(J) A representative plot of the action potentials recorded from a Tdt$^+$ neuron in response to sequential perfusions of AMPA (1 μM), and combination of AMPA (1 μM) and NMB (2 μM) under perforated patch clamp configuration. Raw traces are shown recording at (A, B, C, D, and E) time points.

(K) Quantification of the frequency of action potentials during baseline, AMPA-only perfusion, and AMPA and NMB perfusion together. Data are presented as mean ± SEM. Unpaired Student's t test in (K). *p < 0.05

by our blind recordings and single-cell RT-PCR (Figure S2K). To provide additional evidence supporting monosynaptic connections between MRGPRA3$^+$ primary afferents and NMBR$^+$ DH neurons, we intrathecally injected AAV-PHP.S:CAG-DIO-ChR2-eYFP into *Mrgpra3^{Cre}*; *Nmbr^{Cre}*; *Rosa$^{Tdtf/+}$* mice, in which both *Mrgpra3*$^+$ afferents and *Nmbr*$^+$ DH neurons express Tdt (Figure 6A). Because AAV-PHP.S efficiently transduces peripheral neurons (Chan et al., 2017), only MRGPRA3$^+$ afferents should express ChR2 (Figure 6A). Indeed, whole mount lumbar DRGs and spinal cord sections showed specific expression of ChR2 in MRGPRA3$^+$ primary afferents (Figures 6B–6G). Using spinal cord slice recordings from these mice with repetitive light stimuli, we found monosynaptic connections between MRGPRA3$^+$ afferents and some NMBR$^+$ DH neurons (5/15 neurons recorded, Figures 6H and 6I). To test whether NMB and glutamate might have additive effects on NMBR$^+$ DH neurons, we recorded *Nmbr-Tdt* neurons while perfusing AMPA (α-amino-3-hydroxy-5-methyl-4-isoxazolepropionic acid) and NMB together. We found that glutamate alone can increase the firing rates of *Nmbr-Tdt* neurons transiently (Figure 6J, points b and c), but co-perfusion of AMPA and NMB greatly enhanced the activity of these neurons in a prolonged manner (Figure 6J, points d and e) (action potential frequency at the baseline 2.0 ± 0.5 Hz versus AMPA only 3.4 ± 0.5 Hz versus AMPA and NMB 5.0 ± 0.7 Hz, n = 6, p < 0.05) (Figures 6J and 6K). Together, our results suggest that

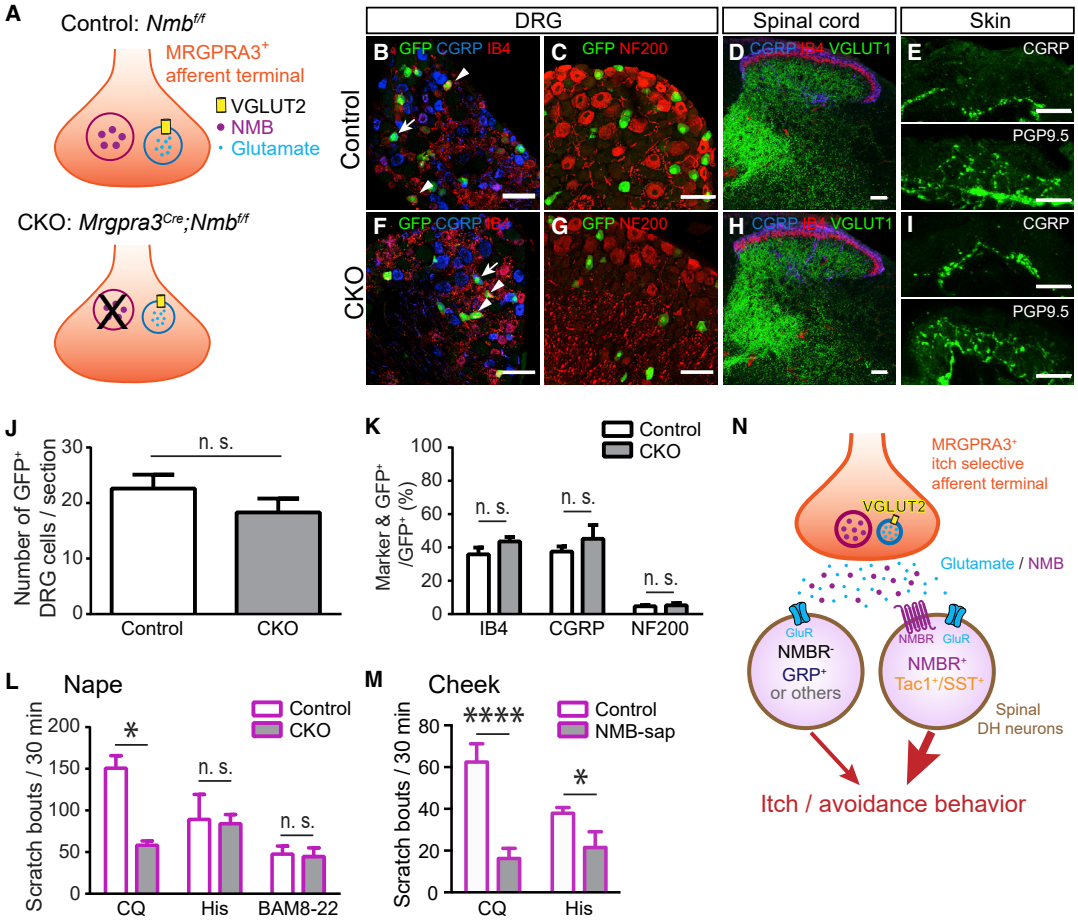

Figure 7. NMB is required in MRGPRA3$^+$ afferents for CQ-induced itch behavior

(A) Illustration showing MRGPRA3$^+$ afferent terminals of *Nmb*$^{f/f}$ (control) and *Mrgpra3*^{Cre}; *Nmb*$^{f/f}$ (*Mrgpra3-Nmb* CKO) mice.

(B–I) Immunostaining of molecular markers with sections from lumbar (L4 and L5) DRG, lumbar spinal cord, and hairy skin of around 2-month-old control and CKO mice. Scale bars: DRG 50 μm, spinal cord 50 μm, skin 10 μm.

(J and K) Quantification of MRGPRA3-GFP$^+$ neurons per sections and percentage of MRGPRA3-GFP$^+$ neurons expressing different molecular markers. 6–8 sections/mouse, n = 3.

(L) Quantification of scratch bouts in response to the nape of neck intradermal injections of CQ or histamine or BAM8-22 into 2-month-old control and *Mrgpra3-Nmb* CKO mice.

(M) Quantification of scratch bouts in response to cheek intradermal injections of CQ or histamine into 2-month-old blank-saporin (control) and NMB-saporin (NMB-sap) mice.

(N) Illustration of the proposed model. See also Figure S7. Unpaired Data are presented as mean ± SEM. Student's t test in (J, K, L, and M). ****$p < 0.001$, *$p < 0.05$; n.s., not significant

MRGPRA3$^+$ afferents may use glutamate and/or NMB to excite postsynaptic NMBR$^+$ neurons.

Nmb in MRGPRA3$^+$ primary afferents and NMBR$^+$ interneurons function in itch behaviors

Finally, to determine how NMB functions in MRGPRA3$^+$ primary afferents to mediate itch behaviors, we generated *MrgprA3-Nmb* CKO (*Mrgpra3*^{Cre}; *Nmb*$^{f/f}$) mice (Figures 7A, S7A, and S7B). Histological examination of DRG, spinal cord, and hairy skin sections from control and CKO mice revealed no gross anatomical differences between the groups (Figures 7B–7I). The number of MRGPRA3$^+$GFP$^+$ cells (control 22.6 ± 2.5 neurons/section versus CKO 18.3 ± 2.5 neurons/section, $p > 0.05$) and the expression of molecular markers within MRGPRA3$^+$GFP$^+$ neurons (IB4$^+$GFP$^+$/GFP$^+$: control 35.9% ± 4.1% versus CKO 43.6% ± 2.7%, $p > 0.05$; CGRP$^+$GFP$^+$/GFP$^+$: control 37.6% ± 3.0% versus CKO 45.2% ± 8.3%, $p > 0.05$; NF200$^+$GFP$^+$/GFP$^+$: control 4.7% ± 0.8% versus CKO 5.3% ± 1.4%, $p > 0.05$) were also comparable (Figures 7J and 7K), suggesting that *Nmb* ablation in MRGPRA3$^+$ afferents does not cause obvious anatomical or molecular marker changes. Interestingly, compared with control mice, *Mrgpra3-Nmb* CKO mice showed a

significant reduction of scratching only in response to nape injection of CQ (control 150.8 ± 15.0 bouts/30 min, n = 5 versus CKO 58.3 ± 5.2 bouts/30 min, n = 6, $p < 0.05$) but not with other tested pruritogens (histamine: control 89.3 ± 29.9 bouts/30 min, n = 6 versus CKO 84.8 ± 11.4 bouts/30 min, n = 6, $p > 0.05$; BAM8-22: control 47.6 ± 9.6 bouts/30 min, n = 5 versus CKO 44.6 ± 10.5 bouts/30 min, n = 5, $p > 0.05$) (Figure 7L). To examine the role of NMBR$^+$ DH neurons, we performed intracisternal injection of NMB-saporin (NMB-sap) into wild-type mice to ablate NMBR$^+$ DH neurons (Li et al., 2021; Mishra et al., 2012; Wan et al., 2017). Mice treated with NMB-sap showed significantly decreased scratching responses to both CQ and histamine cheek injection compared with vehicle-injected control mice (Figure 7M). Together, our results suggest that NMB in MRGPRA3$^+$ primary afferents is used for CQ-induced itch responses, whereas NMBR$^+$ neurons, which integrate both glutamate and NMB signals, function more broadly in itch transmission.

DISCUSSION

Here, we found that transcripts of *Vglut2* and *Nmb*, but not other canonical vesicular glutamate transporters or neuropeptides, are highly expressed in itch-selective MRGPRA3$^+$ primary afferents. MRGPRA3$^+$ afferents form monosynaptic connections with both NMBR$^+$ and NMBR$^-$ DH neurons and use glutamate as an essential neurotransmitter for synaptic transmission and itch behaviors. NMB may directly activate NMBR$^+$ neurons or function together with glutamate to enhance the activities of NMBR$^+$ neurons for itch transmission and behaviors (Figure 7N).

In addition to scratching, we observed that optogenetic stimuli on the cheek and nape of *Mrgpra3-ChR2* mice elicited other avoidance behaviors, such as HS and asymmetric BW. Because itch is an aversive sensation (Su et al., 2019), it is possible that these avoidance responses are part of natural itch-related behaviors in mice. It is noteworthy that the mouse cheek behavioral model for differentiation of nociceptive and itch behaviors was originally established using histamine and capsaicin (Shimada and LaMotte, 2008), and that bilateral wiping was broadly classified as grooming and was not directly quantified. With CQ cheek injection, we observed a preferential increase in asymmetric BW, in which the contralateral forepaw is lifted but not directed toward the cheek (Figures S1I–S1L). On the other hand, capsaicin eye drops elicit an increase in both asymmetric and symmetric bilateral forepaw grooming (Figures S1M and S1N), whereas UW, in which the contralateral forepaw remains on the ground, was rare in response to either stimulus (Figures S1K and S1M). Similar asymmetric bilateral wiping behavior was observed in response to optogenetic/pharmacological activation of MRGPRA3$^+$ afferents (Sharif et al., 2020) and to intrathecal injection of GRP (Sheahan et al., 2020), which activates itch-specific spinal cord interneurons. Together, these studies and our results raise the possibility that BW in mice may be a nociception-associated but not nociception-specific behavior and that it can also be triggered by pruriceptive pathways (Figure S1O). Another possibility is that bilateral wiping specifically indicates nociception and that MRGPRA3$^+$ neurons as well as GRPR$^+$ interneurons signal both nociception and itch in mice. More experiments and discussion will be needed before reaching a consensus for interpreting this behavior. In short, our results indicate that chemical/optical stimulation of MRGPRA3$^+$ afferents activates a combination of downstream circuits, some of which lead to scratching and some of which lead to bilateral wiping and other avoidance behaviors. Because noxious stimuli also trigger wiping and other avoidance behaviors, itch and nociception may share partially overlapping circuits for eliciting a complete cohort of natural behaviors.

Although *Vglut2* is highly expressed in both nociceptive and itch-sensing primary afferents, previous studies have reported that *Vglut2* CKO mice display a reduction of nocifensive behaviors but no change or even an increase in itch behaviors, raising the possibility that glutamate is dispensable for itch transmission (Lagerström et al., 2010; Lagerström et al., 2011; Liu et al., 2010; Ma, 2014; Rogoz et al., 2012; Scherrer et al., 2010). Here, we found that glutamate transmission exhibits an age-dependent reduction in both *Trpv1-Vglut2* and *Mrgpra3-Vglut2* CKO mouse lines. Glutamate reduction in *Trpv1^{Cre}*-positive afferents is significant when these mutant mice are around 8 weeks old, whereas that of *Mrgpra3-Vglut2* CKO mice is significant when they are 6 months old. Whether there is a further temporal delay between a physiologically measurable reduction in glutamatergic transmission and a behavioral change is currently unclear. The mechanism underlying this age-dependent loss-of-function of *Vglut2*, despite our observation that knockout recombination occurs at early postnatal stages, is also elusive. One possibility is that residual full-length VGLUT2 protein can last for several weeks/months in *Vglut2* CKO mice. Compensation from *Vglut1* and *Vglut3* is also plausible but less likely, as we found no evidence of *Vglut1* and *Vglut3* upregulation based on transcript expression. Given that glutamate is still vesicle-dependent in *Vglut2*-ablated afferents, a third possibility is the existence of non-canonical vesicular glutamate transporters, which may serve a compensatory function for different periods of time in different populations of primary afferents. The time when glutamatergic transmission is lost in different populations of primary afferents also helps to understand the increased itch behavior phenotype of *Trpv1-Vglut2* CKO mice. Because the reduction of glutamate transmission in some *Trpv1^{Cre}*-lineage afferents occurs much earlier (~8 weeks) than in MRGPRA3$^+$ afferents (~6 months), a broad ablation of *Vglut2* using *Trpv1^{Cre}* would mainly reveal phenotypes of glutamate loss in nociceptors but not itch-sensing afferents, if the CKO mice were examined at ages younger than 6 months. On the other hand, *Mrgpra3-Vglut2* CKO mice, in which glutamate transmission is lost in itch-selective afferents at 6 months, showed an almost complete abolishment of optical-induced itch behaviors, chemical-induced acute scratching, and spontaneous scratching in a contact dermatitis model. Thus, our experiments provide new evidence that glutamate is not dispensable but rather plays an essential role in itch transmission.

Transcripts of the neuropeptide *Nmb* were highly expressed in MRGPRA3$^+$ itch-selective primary afferents, which exhibit monosynaptic connectivity with NMBR$^+$ DH neurons. We tried optical and electrical stimulation with both blind and targeted *Nmbr-Tdt* neuron recordings (Figures S7C–S7H), but, unfortunately, we could not detect obvious NMB release from MRGPRA3$^+$ or C fibers using our experimental conditions. Although neuropeptides are proposed to function as important

molecular mediators in somatosensory afferents (Ma, 2014; Mishra and Hoon, 2013; Sun et al., 2009), to the best of our knowledge, no previous publication has directly demonstrated synaptic neuropeptide release from primary sensory neurons, likely due to similar technical difficulties. Instead, we showed that NMB perfusion can depolarize NMBR$^+$ DH neurons, NMB and glutamate have additive effects on NMBR$^+$ DH neuron activity, *Nmb* is required in MRGPRA3$^+$ afferents for CQ-induced scratching, and NMBR$^+$ DH neurons function in CQ- and histamine-induced scratching. Together, these data support the role of NMB from MRGPRA3$^+$ afferents in mediating synaptic communication with NMBR$^+$ DH neurons for itch transmission. It is noteworthy that MRGPRA3$^+$ itch-selective afferents also synapse with NMBR$^-$ excitatory DH neurons, some of which are GRP$^+$. GRP$^+$ interneurons are excitatory interneurons downstream of MRGPRA3$^+$ afferents and play important roles in itch transmission (Pagani et al., 2019; Sun et al., 2017).

In short, our findings provide supportive evidence that both glutamate and NMB in MRGPRA3$^+$ afferents play a role in synaptic transmission and itch sensation/behavior. However, because glutamate is used by almost all primary somatosensory afferents and *Nmb* is broadly expressed in itch-sensing and nociceptive afferents (Fleming et al., 2012), these results do not corroborate the "itch-selective neurotransmitter" model. Instead, we propose that particular neural circuits activated by a given population of primary afferents, rather than the particular set of neurotransmitters they use, dictate sensory modality specificity and behavioral output.

STAR★METHODS

Detailed methods are provided in the online version of this paper and include the following:

- KEY RESOURCES TABLE
- RESOURCE AVAILABILITY
  - Lead contact
  - Materials availability
  - Data and code availability
- EXPERIMENTAL MODEL AND SUBJECT DETAILS
- METHOD DETAILS
  - *In Situ* Hybridization
  - Immunohistochemistry
  - Intrathecal AAV and NMB-Saporin Injections
  - Electrophysiology and Optogenetics
  - Reverse Transcription Polymerase Chain Reaction (RT-PCR)
  - Itch Behavior Assays
  - High-Speed Imaging
  - Mechanosensitivity and Thermal Sensitivity Behavior Assays
  - Image Acquisition
- QUANTIFICATION AND STATISTICAL ANALYSIS

SUPPLEMENTAL INFORMATION

Supplemental information can be found online at https://doi.org/10.1016/j.neuron.2021.12.007.

ACKNOWLEDGMENTS

We thank Dr. Yulong Li at Peking University for his insightful suggestions on experimental design. We thank the Johns Hopkins Transgenic Core for generating the *Nmbr*^{Cre} knockin mouse line and the Penn Skin Biology and Disease Resource-Based Center (Penn SBDRC) core facility for sectioning mouse skin samples. We thank Yi Gu at the National Institute of Neurological Disorders and Stroke as well as lab members in the Liu, Luo, and Ma labs for their help with the manuscript. This work is supported by NIH R01 grants (AI125743, AI163146, and EY024704) to Q.L. and NIH R01 grants (NS083702 and NS094224) to W.L.

AUTHOR CONTRIBUTIONS

Conceptualization, L.C., M.M., Q.L., and W.L.; methodology, L.C., J.G., M.M., T.R., Q.L., and W.L.; investigation, L.C., J.G., S.L.C., M.G., J.B., K.B. W.O., R.C.C., Q.W., and X.S.; writing—original draft, L.C., S.L.C., and W.L.; writing—review and editing, L.C., S.L.C., M.M., Q.L., and W.L.; funding acquisition, Q.L. and W.L.; resources, W.L., Q.L., M.M., and V.G.; supervision, M.M., Q.L., and W.L.

DECLARATION OF INTERESTS

V.G. is a member of the Neuron Advisory Board. V.G. is also a cofounder and board member of Capsida Biotherapeutics, a fully integrated AAV engineering and gene therapy company. The other authors declare no competing interests.

INCLUSION AND DIVERSITY

We worked to ensure sex balance in the selection of non-human subjects. One or more of the authors of this paper self-identifies as a member of the LGBTQ+ community.

Received: June 8, 2020
Revised: August 21, 2021
Accepted: December 6, 2021
Published: January 4, 2022

REFERENCES

Abdus-Saboor, I., Fried, N.T., Lay, M., Burdge, J., Swanson, K., Fischer, R., Jones, J., Dong, P., Cai, W., Guo, X., et al. (2019). Development of a mouse pain scale using sub-second behavioral mapping and statistical modeling. Cell Rep *28*, 1623–1634.e4.

Albisetti, G.W., Pagani, M., Platonova, E., Hösli, L., Johannssen, H.C., Fritschy, J.M., Wildner, H., and Zeilhofer, H.U. (2019). Dorsal horn gastrin-releasing peptide expressing neurons transmit spinal itch but not pain signals. J. Neurosci. *39*, 2238–2250.

Alshahrani, S., Fernandez-Conti, F., Araujo, A., and DiFulvio, M. (2012). Rapid determination of the thermal nociceptive threshold in diabetic rats. J. Vis. Exp. *63*, e3785.

Bautista, D.M., Wilson, S.R., and Hoon, M.A. (2014). Why we scratch an itch: the molecules, cells and circuits of itch. Nat. Neurosci. *17*, 175–182.

Carstens, E. (2016). Many parallels between itch and pain research. Eur. J. Pain *20*, 5–7.

Carstens, E.E., Carstens, M.I., Simons, C.T., and Jinks, S.L. (2010). Dorsal horn neurons expressing NK-1 receptors mediate scratching in rats. Neuroreport *21*, 303–308.

Cavanaugh, D.J., Chesler, A.T., Jackson, A.C., Sigal, Y.M., Yamanaka, H., Grant, R., O'Donnell, D., Nicoll, R.A., Shah, N.M., Julius, D., and Basbaum, A.I. (2011). Trpv1 reporter mice reveal highly restricted brain distribution and functional expression in arteriolar smooth muscle cells. J. Neurosci. *31*, 5067–5077.

Challis, R.C., Ravindra Kumar, S., Chan, K.Y., Challis, C., Beadle, K., Jang, M.J., Kim, H.M., Rajendran, P.S., Tompkins, J.D., Shivkumar, K., et al.

(2019). Systemic AAV vectors for widespread and targeted gene delivery in rodents. Nat. Protoc. *14*, 379–414.

Chan, K.Y., Jang, M.J., Yoo, B.B., Greenbaum, A., Ravi, N., Wu, W.-L., Sánchez-Guardado, L., Lois, C., Mazmanian, S.K., Deverman, B.E., and Gradinaru, V. (2017). Engineered AAVs for efficient noninvasive gene delivery to the central and peripheral nervous systems. Nat. Neurosci. *20*, 1172–1179.

Chaplan, S.R., Bach, F.W., Pogrel, J.W., Chung, J.M., and Yaksh, T.L. (1994). Quantitative assessment of tactile allodynia in the rat paw. J. Neurosci. Methods *53*, 55–63.

Chen, X.-J., and Sun, Y.-G. (2020). Central circuit mechanisms of itch. Nat. Commun. *11*, 3052.

Cheng, L., Duan, B., Huang, T., Zhang, Y., Chen, Y., Britz, O., Garcia-Campmany, L., Ren, X., Vong, L., Lowell, B.B., et al. (2017). Identification of spinal circuits involved in touch-evoked dynamic mechanical pain. Nat. Neurosci. *20*, 804–814.

Chiu, I.M., Barrett, L.B., Williams, E.K., Strochlic, D.E., Lee, S., Weyer, A.D., Lou, S., Bryman, G.S., Roberson, D.P., Ghasemlou, N., et al. (2014). Transcriptional profiling at whole population and single cell levels reveals somatosensory neuron molecular diversity. Elife *3*, e04660.

Cui, L., Miao, X., Liang, L., Abdus-Saboor, I., Olson, W., Fleming, M.S., Ma, M., Tao, Y.-X., and Luo, W. (2016). Identification of early RET+ deep dorsal spinal cord interneurons in gating pain. Neuron *91*, 1137–1153.

Dong, P., Guo, C., Huang, S., Ma, M., Liu, Q., and Luo, W. (2017). TRPC3 is dispensable for beta-alanine triggered acute itch. Sci. Rep. *7*, 13869.

Dong, X., and Dong, X. (2018). Peripheral and central mechanisms of itch. Neuron *98*, 482–494.

Doyle, M.W., and Andresen, M.C. (2001). Reliability of monosynaptic sensory transmission in brain stem neurons in vitro. J. Neurophysiol. *85*, 2213–2223.

Dröse, S., and Altendorf, K. (1997). Bafilomycins and concanamycins as inhibitors of V-ATPases and P-ATPases. J. Exp. Biol. *200*, 1–8.

Fleming, M.S., Ramos, D., Han, S.B., Zhao, J., Son, Y.-J., and Luo, W. (2012). The majority of dorsal spinal cord gastrin releasing peptide is synthesized locally whereas neuromedin B is highly expressed in pain- and itch-sensing somatosensory neurons. Mol. Pain *8*, 52.

Fleming, M.S., Vysochan, A., Paixão, S., Niu, J., Klein, R., Savitt, J.M., and Luo, W. (2015). Cis and trans RET signaling control the survival and central projection growth of rapidly adapting mechanoreceptors. Elife *4*, e06828.

Goswami, S.C., Thierry-Mieg, D., Thierry-Mieg, J., Mishra, S., Hoon, M.A., Mannes, A.J., and Iadarola, M.J. (2014). Itch-associated peptides: RNA-Seq and bioinformatic analysis of natriuretic precursor peptide B and gastrin releasing peptide in dorsal root and trigeminal ganglia, and the spinal cord. Mol. Pain *10*, 44.

Han, L., Ma, C., Liu, Q., Weng, H.-J., Cui, Y., Tang, Z., Kim, Y., Nie, H., Qu, L., Patel, K.N., et al. (2013). A subpopulation of nociceptors specifically linked to itch. Nat. Neurosci. *16*, 174–182.

Häring, M., Zeisel, A., Hochgerner, H., Rinwa, P., Jakobsson, J.E.T., Lönnerberg, P., La Manno, G., Sharma, N., Borgius, L., Kiehn, O., et al. (2018). Neuronal atlas of the dorsal horn defines its architecture and links sensory input to transcriptional cell types. Nat. Neurosci. *21*, 869–880.

Ikoma, A., Steinhoff, M., Ständer, S., Yosipovitch, G., and Schmelz, M. (2006). The neurobiology of itch. Nat. Rev. Neurosci. *7*, 535–547.

Kiguchi, N., Uta, D., Ding, H., Uchida, H., Saika, F., Matsuzaki, S., Fukazawa, Y., Abe, M., Sakimura, K., Ko, M.-C., and Kishioka, S. (2020). GRP receptor and AMPA receptor cooperatively regulate itch-responsive neurons in the spinal dorsal horn. Neuropharmacology *170*, 108025.

Lagerström, M.C., Rogoz, K., Abrahamsen, B., Lind, A.L., Olund, C., Smith, C., Mendez, J.A., Wallén-Mackenzie, Å., Wood, J.N., and Kullander, K. (2011). A sensory subpopulation depends on vesicular glutamate transporter 2 for mechanical pain, and together with substance P, inflammatory pain. Proc. Natl. Acad. Sci. USA *108*, 5789–5794.

Lagerström, M.C., Rogoz, K., Abrahamsen, B., Persson, E., Reinius, B., Nordenankar, K., Olund, C., Smith, C., Mendez, J.A., Chen, Z.-F., et al. (2010). VGLUT2-dependent sensory neurons in the TRPV1 population regulate pain and itch. Neuron *68*, 529–542.

Li, C., Wang, S., Chen, Y., and Zhang, X. (2018). Somatosensory neuron typing with high-coverage single-cell RNA sequencing and functional analysis. Neurosci. Bull. *34*, 200–207.

Li, C.-L., Li, K.-C., Wu, D., Chen, Y., Luo, H., Zhao, J.-R., Wang, S.-S., Sun, M.-M., Lu, Y.-J., Zhong, Y.-Q., et al. (2016). Somatosensory neuron types identified by high-coverage single-cell RNA-sequencing and functional heterogeneity. Cell Res *26*, 83–102.

Li, F., Jiang, H., Shen, X., Yang, W., Guo, C., Wang, Z., Xiao, M., Cui, L., Luo, W., Kim, B.S., et al. (2021). Sneezing reflex is mediated by a peptidergic pathway from nose to brainstem. Cell *184*, 3762–3773.e10.

Liu, Q., Sikand, P., Ma, C., Tang, Z., Han, L., Li, Z., Sun, S., LaMotte, R.H., and Dong, X. (2012). Mechanisms of itch evoked by beta-alanine. J. Neurosci. *32*, 14532–14537.

Liu, Y., Abdel Samad, O., Zhang, L., Duan, B., Tong, Q., Lopes, C., Ji, R.-R., Lowell, B.B., and Ma, Q. (2010). VGLUT2-dependent glutamate release from nociceptors is required to sense pain and suppress itch. Neuron *68*, 543–556.

Liu, Q., Tang, Z., Surdenikova, L., Kim, S., Patel, K.N., Kim, A., Ru, F., Guan, Y., Weng, H.-J., Geng, Y., et al. (2009). Sensory neuron-specific GPCR Mrgprs are itch receptors mediating chloroquine-induced pruritus. Cell *139*, 1353–1365.

Ma, Q. (2014). Itch modulation by VGLUT2-dependent glutamate release from somatic sensory neurons. In Itch: Mechanisms and Treatment, E. Carstens and T. Akiyama, eds. (CRC Press/Taylor & Francis).

Madisen, L., Zwingman, T.A., Sunkin, S.M., Oh, S.W., Zariwala, H.A., Gu, H., Ng, L.L., Palmiter, R.D., Hawrylycz, M.J., Jones, A.R., et al. (2010). A robust and high-throughput Cre reporting and characterization system for the whole mouse brain. Nat. Neurosci. *13*, 133–140.

Mishra, S.K., Holzman, S., and Hoon, M.A. (2012). A nociceptive signaling role for neuromedin B. J. Neurosci. *32*, 8686–8695.

Mishra, S.K., and Hoon, M.A. (2013). The cells and circuitry for itch responses in mice. Science *340*, 968–971.

Mnyika, K.S., and Kihamia, C.M. (1991). Chloroquine-induced pruritus: its impact on chloroquine utilization in malaria control in Dar es Salaam. J. Trop. Med. Hyg. *94*, 27–31.

Nguyen, M.Q., Wu, Y., Bonilla, L.S., von Buchholtz, L.J., and Ryba, N.J.P. (2017). Diversity amongst trigeminal neurons revealed by high throughput single cell sequencing. PloS One *12*, e0185543.

Olson, W., Abdus-Saboor, I., Cui, L., Burdge, J., Raabe, T., Ma, M., and Luo, W. (2017). Sparse genetic tracing reveals regionally specific functional organization of mammalian nociceptors. Elife *6*, e29507.

Pagani, M., Albisetti, G.W., Sivakumar, N., Wildner, H., Santello, M., Johannssen, H.C., and Zeilhofer, H.U. (2019). How gastrin-releasing peptide opens the spinal gate for itch. Neuron *103*, 102–117.e5.

Park, S.A., Yang, E.J., Han, S.K., and Park, S.J. (2012). Age-related changes in the effects of 5-hydroxytryptamine on substantia gelatinosa neurons of the trigeminal subnucleus caudalis. Neurosci. Lett. *510*, 78–81.

Pereira, M.P., and Ständer, S. (2017). Assessment of severity and burden of pruritus. Allergol. Int. *66*, 3–7.

Qu, L., Fan, N., Ma, C., Wang, T., Han, L., Fu, K., Wang, Y., Shimada, S.G., Dong, X., and LaMotte, R.H. (2014). Enhanced excitability of MRGPRA3- and MRGPRD-positive nociceptors in a model of inflammatory itch and pain. Brain *137*, 1039–1050.

Roccaro-Waldmeyer, D.M., Girard, F., Milani, D., Vannoni, E., Prétôt, L., Wolfer, D.P., and Celio, M.R. (2018). Eliminating the VGlut2-dependent glutamatergic transmission of parvalbumin-expressing neurons leads to deficits in locomotion and vocalization, decreased pain sensitivity, and increased dominance. Front. Behav. Neurosci. *12*, 146.

Rogoz, K., Lagerström, M.C., Dufour, S., and Kullander, K. (2012). VGLUT2-dependent glutamatergic transmission in primary afferents is required for intact nociception in both acute and persistent pain modalities. Pain *153*, 1525–1536.

Santos, S.F., Rebelo, S., Derkach, V.A., and Safronov, B.V. (2007). Excitatory interneurons dominate sensory processing in the spinal substantia gelatinosa of rat. J. Physiol. *581*, 241–254.

Scherrer, G., Low, S.A., Wang, X., Zhang, J., Yamanaka, H., Urban, R., Solorzano, C., Harper, B., Hnasko, T.S., Edwards, R.H., and Basbaum, A.I. (2010). VGLUT2 expression in primary afferent neurons is essential for normal acute pain and injury-induced heat hypersensitivity. Proc. Natl. Acad. Sci. USA *107*, 22296–22301.

Scott, A.E., Kashon, M.L., Yucesoy, B., Luster, M.I., and Tinkle, S.S. (2002). Insights into the quantitative relationship between sensitization and challenge for allergic contact dermatitis reactions. Toxicol. Appl. Pharmacol. *183*, 66–70.

Sharif, B., Ase, A.R., Ribeiro-da-Silva, A., and Séguéla, P. (2020). Differential coding of itch and pain by a subpopulation of primary afferent neurons. Neuron *106*, 940–951.e4.

Sheahan, T.D., Warwick, C.A., Fanien, L.G., and Ross, S.E. (2020). The Neurokinin-1 receptor is expressed with gastrin-releasing peptide receptor in spinal interneurons and modulates itch. J. Neurosci. *40*, 8816–8830.

Shimada, S.G., and LaMotte, R.H. (2008). Behavioral differentiation between itch and pain in mouse. Pain *139*, 681–687.

Solinski, H.J., Kriegbaum, M.C., Tseng, P.-Y., Earnest, T.W., Gu, X., Barik, A., Chesler, A.T., and Hoon, M.A. (2019). Nppb neurons are sensors of mast cell-induced itch. Cell Rep *26*, 3561–3573.e4.

Solorzano, C., Villafuerte, D., Meda, K., Cevikbas, F., Bráz, J., Sharif-Naeini, R., Juarez-Salinas, D., Llewellyn-Smith, I.J., Guan, Z., and Basbaum, A.I. (2015). Primary afferent and spinal cord expression of gastrin-releasing peptide: message, protein, and antibody concerns. J. Neurosci. *35*, 648–657.

Ständer, S., Weisshaar, E., Mettang, T., Szepietowski, J.C., Carstens, E., Ikoma, A., Bergasa, N.V., Gieler, U., Misery, L., Wallengren, J., et al. (2007). Clinical classification of itch: a position paper of the International Forum for the Study of Itch. Acta Derm. Venereol. *87*, 291–294.

Su, P.-Y., and Ko, M.-C. (2011). The role of central gastrin-releasing peptide and neuromedin B receptors in the modulation of scratching behavior in rats. J. Pharmacol. Exp. Ther. *337*, 822–829.

Su, X.-Y., Chen, M., Yuan, Y., Li, Y., Guo, S.-S., Luo, H.-Q., Huang, C., Sun, W., Li, Y., Zhu, M.X., et al. (2019). Central processing of itch in the midbrain reward center. Neuron *102*, 858–872.e5.

Sun, S., Xu, Q., Guo, C., Guan, Y., Liu, Q., and Dong, X. (2017). Leaky gate model: intensity-dependent coding of pain and itch in the spinal cord. Neuron *93*, 840–853.e5.

Sun, Y.-G., and Chen, Z.-F. (2007). A gastrin-releasing peptide receptor mediates the itch sensation in the spinal cord. Nature *448*, 700–703.

Sun, Y.-G., Zhao, Z.-Q., Meng, X.-L., Yin, J., Liu, X.-Y., and Chen, Z.-F. (2009). Cellular basis of itch sensation. Science *325*, 1531–1534.

Ting, J.T., Daigle, T.L., Chen, Q., and Feng, G. (2014). Acute brain slice methods for adult and aging animals: application of targeted patch clamp analysis and optogenetics. Methods Mol. Biol. *1183*, 221–242.

Tong, Q., Ye, C., McCrimmon, R.J., Dhillon, H., Choi, B., Kramer, M.D., Yu, J., Yang, Z., Christiansen, L.M., Lee, C.E., et al. (2007). Synaptic glutamate release by ventromedial hypothalamic neurons is part of the neurocircuitry that prevents hypoglycemia. Cell Metab *5*, 383–393.

Usoskin, D., Furlan, A., Islam, S., Abdo, H., Lönnerberg, P., Lou, D., Hjerling-Leffler, J., Haeggström, J., Kharchenko, O., Kharchenko, P.V., et al. (2015). Unbiased classification of sensory neuron types by large-scale single-cell RNA sequencing. Nat. Neurosci. *18*, 145–153.

Wallace, M.L., Saunders, A., Huang, K.W., Philson, A.C., Goldman, M., Macosko, E.Z., McCarroll, S.A., and Sabatini, B.L. (2017). Genetically distinct parallel pathways in the entopeduncular nucleus for limbic and sensorimotor output of the basal ganglia. Neuron *94*, 138–152.e5.

Wan, L., Jin, H., Liu, X.-Y., Jeffry, J., Barry, D.M., Shen, K.-F., Peng, J.-H., Liu, X.-T., Jin, J.-H., Sun, Y., et al. (2017). Distinct roles of NMB and GRP in itch transmission. Sci. Rep. *7*, 15466.

Wang, F., Flanagan, J., Su, N., Wang, L.-C., Bui, S., Nielson, A., Wu, X., Vo, H.-T., Ma, X.-J., and Luo, Y. (2012). RNAscope: a novel in situ RNA analysis platform for formalin-fixed, paraffin-embedded tissues. J. Mol. Diagn. *14*, 22–29.

Wang, H., and Zylka, M.J. (2009). Mrgprd-expressing polymodal nociceptive neurons innervate most known classes of substantia gelatinosa neurons. J. Neurosci. *29*, 13202–13209.

Weng, Y.-L., An, R., Cassin, J., Joseph, J., Mi, R., Wang, C., Zhong, C., Jin, S.-G., Pfeifer, G.P., Bellacosa, A., et al. (2017). An intrinsic epigenetic barrier for functional axon regeneration. Neuron *94*, 337–346.e6.

Yasaka, T., Tiong, S.Y.X., Hughes, D.I., Riddell, J.S., and Todd, A.J. (2010). Populations of inhibitory and excitatory interneurons in lamina II of the adult rat spinal dorsal horn revealed by a combined electrophysiological and anatomical approach. Pain *151*, 475–488.

Zhu, Y., Hanson, C.E., Liu, Q., and Han, L. (2017). Mrgprs activation is required for chronic itch conditions in mice. Itch (Phila) *2*, e9.

STAR★METHODS

KEY RESOURCES TABLE

REAGENT or RESOURCE	SOURCE	IDENTIFIER
Antibodies		
Chicken polyclonal anti-GFP	Aves Labs	Cat# GFP-1020; RRID:AB_10000240
Rabbit polyclonal anti-GFP	Invitrogen	Cat# A-11122; RRID:AB_221569
Rabbit polyclonal anti-CGRP	ImmunoStar	Cat# 24112; RRID:AB_572217
Rabbit polyclonal anti-PGP9.5	Cedarlane	Cat# CL7756AP; RRID:AB_2792979
Rabbit polyclonal anti-NF200	Sigma-Aldrich	Cat# N4142; RRID:AB_477272
Guinea pig polyclonal anti-VGLUT1	Millipore	Cat# AB5905; RRID:AB_2301751
IB4, Alexa Fluor 488 conjugate	Invitrogen	Cat# I21411; RRID:AB_2314662
IB4, Alexa Fluor 594 conjugate	Invitrogen	Cat# I21413; RRID:AB_2313921
Goat anti-rabbit IgG (H+L), Alexa Fluor 488	Thermo Fisher Scientific	Cat# A-11008; RRID:AB_143165
Goat anti-rabbit IgG (H+L), Alexa Fluor 594	Thermo Fisher Scientific	Cat# A-11012; RRID:AB_2534079
Goat anti-rabbit IgG (H+L), Alexa Fluor 647	Thermo Fisher Scientific	Cat# A-21244; RRID:AB_2535812
Goat anti-chicken IgY (H+L), Alexa Fluor 647	Thermo Fisher Scientific	Cat# A-21449; RRID:AB_2535866
Bacterial and Virus Strains		
AAV-PHP.S:CAG-DIO-ChR2-eYFP	Dr. Viviana Gradinaru	N/A
Chemicals, Peptides, and Recombinant Proteins		
Hematoxylin solution	Sigma-Aldrich	Cat# GHS116
Eosin Y solution	Sigma-Aldrich	Cat# HT110116
NMB-saporin	Advanced Targeting Systems	Cat# IT-70-25
Bafilomycin A1	Tocris	Cat# 13-314-0U; CAS 88899-55-2
NBQX disodium salt	Tocris	Cat# 1044; CAS 479347-86-9
DL-AP5	Tocris	Cat# 0105; CAS 76326-31-3
Tetrodotoxin	Tocris	Cat# 1078; CAS 4368-28-9
Chloroquine disphosphate salt	Sigma Aldrich	Cat# C6628; CAS 50-63-5
SLIGRL-NH_2	R&D Systems	Cat# 1468; CAS 171436-38-7
BAM (8-22)	R&D Systems	Cat# 1763; CAS 412961-36-5
Serotonin hydrochloride	Sigma-Aldrich	Cat# H9523; CAS 153-98-0
Histamine dihydrochloride	Sigma-Aldrich	Cat# H7250; CAS 56-92-8
3,4-Dibutoxy-3-cyclobutene-1,2-dione	Sigma-Aldrich	Cat# 3339792; CAS 2892-62-8
Critical Commercial Assays		
RNAscope Fluorescent Multiplex Reagent Kit	ACD	Cat# 320850
SuperScript First-Strand Synthesis System for RT-PCR	Invitrogen	Cat# 1190418
Deposited Data		
Mouse DRG neuron transcriptome analysis (Chiu et al., 2014)	NCBI Gene Expression Omnibus	GSE55114
Mouse DRG neuron transcriptome analysis (Li et al., 2016)	NCBI Gene Expression Omnibus	GSE63576
Mouse DRG neuron transcriptome analysis (Usoskin et al., 2015)	NCBI Gene Expression Omnibus	GSE59739
Experimental Models: Organisms/Strains		
Mouse: $Mrgpra3^{Cre\text{-}EGFP}$	Dr. Xinzhong Dong	N/A
Mouse: $Vglut2^{f/f}$	Jackson Laboratory	RRID:IMSR_JAX:012898

(*Continued on next page*)

Continued

REAGENT or RESOURCE	SOURCE	IDENTIFIER
Mouse: Rosa$^{Tdtf/f}$	Jackson Laboratory	RRID:IMSR_JAX:007909
Mouse: Nmbr^{Cre}	Drs. Wenqin Luo/Minghong Ma	N/A
Mouse: Trpv1^{Cre}	Jackson Laboratory	RRID:IMSR_JAX:017769
Mouse: Rosa$^{ChR2f/f}$	Jackson Laboratory	RRID:IMSR_JAX:012569
Oligonucleotides		
RT-PCR primers	See Table S3	
Mm-Nmbr-C2 probe	ACD	Cat# 406461-C2
Mm-GRP probe	ACD	Cat# 317861
Mm-Slc32a1 probe	ACD	Cat# 319191
Mm-Slc17a6-C2 probe	ACD	Cat# 319171-C2
Mm-Npr1-C3 probe	ACD	Cat# 484531-C3
Mm-Grpr-C2 probe	ACD	Cat# 3171871-C2
tdTomato and tdTomato-C3 probes	ACD	Cat# 317041/317041-C3
Mm-Tacr1-C3 probe	ACD	Cat# 428781-C3
Mm-Tac1-C3 probe	ACD	Cat# 410351-C3
Software and Algorithms		
FASTCAM Viewer 4	Photron	N/A
Prism 7	GraphPad	RRID:SCR_002798
Fiji	NIH	RRID:SCR_002285
Pulse Software	HEKA Elektronik	N/A
Igor Pro 6	Wavematrics	RRID:SCR_000325
Origin	OriginLab	RRID:SCR_014212
Illustrator	Adobe	RRID:SCR_014198
Other		
FASTCAM Mini UX100	Photron	N/A
Zoom Wide Angle Telephoto 24-85mm f2.8	Nikon	N/A
473 nm blue laser	Shanghai Laser and Optics Century	Cat# BL473T8-150FC
473 nm blue laser	Blue Sky Research	Cat# FTEC2473-V65YF0
Von Frey filaments	Stoelting	Cat# 58011
Hot plate analgesia meter	IITC Life Science	Cat# 39
Hargreaves apparatus	UCSD Instruments	N/A

RESOURCE AVAILABILITY

Lead contact

Further information and requests for resources and reagents should be directed to and will be fulfilled by the lead contact, Wenqin Luo (luow@pennmedicine.upenn.edu).

Materials availability

Materials are available upon request. Mouse lines generated in this study will be deposited to The Jackson Laboratory.

Data and code availability

All data reported in this paper will be shared by the lead contact upon request.

This paper does not report original code.

Any additional information required to reanalyze the data reported in this paper is available from the lead contact upon request.

EXPERIMENTAL MODEL AND SUBJECT DETAILS

Mrgpra3$^{Cre\text{-}EGFP}$ mice (Han et al., 2013) were imported from Dr. Qin Liu's lab at the Washington University School of Medicine to Dr. Luo's lab at the University of Pennsylvania. *Rosa*$^{ChR2f/f}$ (JAX 012569), *Vglut2*$^{f/f}$ (JAX 012898) (Tong et al., 2007), *Trpv1*^{Cre} (JAX 017769)

(Cavanaugh et al., 2011), and *Rosa*$^{Tdtf/f}$ (JAX 007909) (Madisen et al., 2010) mice were purchased from the Jackson Laboratories. The *Nmbr*^{Cre} knock-in mouse line was generated by Dr. Janardhan Bhattarai in the lab, using mouse fertilized oocyte injection of CRISPR/CAS9 mixture conducted by the Johns Hopkins Transgenic Core (details of this mouse line generation will be published in another manuscript). Animals were housed in facilities at the University of Pennsylvania and at the Washington University School of Medicine. All experiments were conducted in accordance with the National Institute of Health guidelines and with approval from the Institutional Animal Care and Use Committee of University of Pennsylvania and Washington University School of Medicine. Adult male and female mice with desired genotypes were kept in a standard 12-h light/dark cycle, with water and food pellets available *ad libitum*. Litters and animals were randomized at the time of assigning experimental conditions for the whole study.

METHOD DETAILS

In Situ Hybridization

All cRNA probes used in this study (*Nmb*, *Tac1, Nppb, Calca, and Vglut1-3*) have been described in the Allen Brain Atlas and were conjugated with either digoxigenin (DIG) or fluorescein isothiocyanate (FITC) (Roche). For tissue preparation to perform RNA *in situ* hybridization, intact spinal columns were dissected from CO2 euthanized mice and rapidly frozen in OCT on a dry-ice/ethanol bath. 20 μm cryosections were collected on Superfrost Plus slides (Fisher, 22-034-979) and allowed to dry for at least 2 hours at room temperature. All steps prior to hybridization were carried out under RNase-free conditions. Double fluorescent *in situ* hybridization (FISH) was performed as previously described (Fleming et al., 2012; Olson et al., 2017). RNAscope probes, Mm-Nmbr-C2 (406461-C2), Mm-Grp (317861), Mm-Slc32a1 (319191), Mm-Slc17a6-C2 (319171-C2), Mm-Npr1-C3 (484531-C3), Mm-Grpr-C2 (317871-C2), tdTomato-C3 (317041-C3), tdTomato (317041), Mm-Tacr1-C3 (428781-C3), and Mm-Tac1-C3 (410351-C3) were purchased from ACD (Advanced Cell Diagnostics, Inc.). *In situ* hybridization was performed according to the RNAScope® 2.0 Fluorescent Multiple Kit User Manual for Fresh Frozen Tissue (Wang et al., 2012).

Immunohistochemistry

Ketamine/xylazine/acepromazine cocktail anesthetized mice were transcardially perfused with 4% PFA in phosphate buffer solution (PBS). Intact lumbar spinal columns, DRG, and skin from the nape of the neck were dissected and post-fixed for 2-4 hours in 4% PFA in PBS at 4°C, cryoprotected in 30% sucrose in PBS O/N at 4°C, and embedded in OCT. 20 μm cryosections of spinal cord, DRG, or skin were collected on Superfrost Plus slides, and allowed to dry at room temperature for at least two hours. Sections were washed in PBT (3X 10 minutes), and then blocked in PBS containing 5% lamb serum and 0.2% TritonX-100 for 1 hour at room temperature. Primary antibodies were diluted in the same buffer, and incubated O/N at 4°C, then washed in PBT (3x10 minutes). Secondary antibodies were incubated in blocking buffer at 1:500 dilution for one hour at room temperature. Slides were then washed in PBT (3x10 minutes) and mounted with Fluormount. Primary antibodies used include chicken anti-GFP (1:1,000; Aves, GFP-1020), rabbit anti-GFP (1:1,000, Invitrogen, A-11122), rabbit anti-CGRP (1:5,000; Immunostar, 24112), rabbit anti-PGP9.5 (1:2,000; Ultra Clone, RA95101), rabbit anti-NF200 (1:2,000; Sigma, N4142), guinea pig anti-VGLUT1 (1:1,000, Millipore, AB5905), and Alexa 488 or 594 conjugated IB4 (1:200; Invitrogen, I21411). Anti-GFP antibodies are used to label the expression of GFP in *Mrgpra3*$^{GFP\text{-}Cre}$ mice or EYFP in *Rosa*$^{ChR2\text{-}EYFP}$ mice. Secondary antibodies are Alexa 488, Alexa 594, or Alexa 647 conjugated goat anti-rabbit antibody, Alexa 647 conjugated goat anti-chicken antibody, and Alexa 647 conjugated goat anti-guinea pig antibody. Secondary antibodies were purchased from Invitrogen or the Jackson Immunoresearch. For hematoxylin and eosin staining, nape skin was collected and fixed in 4% PFA in PBS, dehydrated in 30% sucrose, and embedded in OCT. 20 μm cryosections were collected on Superfrost Plus slides, and hematoxylin (GHS116) and eosin (HT110116) (H&E) staining was performed according to standard protocols.

Intrathecal AAV and NMB-Saporin Injections

For intrathecal injection of AAV-PHP.S:CAG-DIO-ChR2-eYFP (1.53x10^{10} vector genomes/μl, produced in V. Gradinaru lab (California Institute of Technology) as previously described (Challis et al., 2019)), four-week-old *Mrgpra3*^{Cre}*; Nmbr*^{Cre}*; Rosa*$^{Tdtf/f}$ mice were anesthetized and shaved to expose the skin around the lumbar region. 5 μl of viral solution was injected into the cerebrospinal fluid between vertebrae L5 and L6 using a 30-gauge Hamilton syringe (Weng et al., 2017). Recordings were done 3 weeks after injection to ensure substantial viral expression in DRG. To ablate NMBR^{+} DH neurons, four- to five-week-old C57BL/6J mice were anesthetized using a ketamine/xylazine cocktail (Putney, B4N4) and restrained inside a custom-made injection apparatus (Li et al., 2021). The heads were immobilized at a slight downward angle to expose the atlanto-occipital joint. 3 μg (5 μl volume) of NMB-saporin (Advanced Targeting Systems, IT-70-25) in saline was then injected into the cleft using a 30-gauge Hamilton syringe. Control mice were injected with unconjugated saporin (blank-saporin). Animals were used for behavioral experiments 3 weeks after injection.

Electrophysiology and Optogenetics

Mice between one and six months of age were anesthetized with a ketamine/xylazine/acepromazine cocktail. Laminectomy was performed, and spinal cord lumbar segments were removed and placed in ice-cold NMDG aCSF solution (Ting et al., 2014). 400–500 μm thick transverse spinal cord slices were prepared using a VT1200S vibratome (Leica Microsystems, Nussloch, Germany) and incubated in carbogenated NMDG aCSF solution for 10 min at 32-34°C. Slices were transferred into room-temperature HEPES holding aCSF under constant carbogenation for 1–5 hours before use. The recording solution consisted of (in mM) 127 NaCl, 1.8 KCl, 1.2

KH_2PO_4, 2.4 $CaCl_2$, 1.3 $MgSO_4$, 26 $NaHCO_3$, and 15 glucose at a pH of 7.35–7.45, and an osmolality of 300–310 mOsm. The slices were transferred to the recording chamber and continuously perfused with recording solution at a rate of 3-4 ml/min. Recordings were performed at RT. Spinal cord slices were visualized with an Olympus BX 61WI microscope (Olympus Optical, Tokyo, Japan), and the substantia gelatinosa (lamina II), which is a translucent band across the dorsal horn, was used as a landmark. In the whole cell patch-clamp configuration, glass pipettes (3–5 MΩ) were filled with internal solution consisting of (in mM) 120 K-gluconate, 10 KCl, 2 MgATP, 0.5 NaGTP, 20 HEPES, 0.5 EGTA, and 10 phosphocreatine di(tris) salt at a pH of 7.29 and an osmolality of 300mOsm. For perforated patch recording, the tip of glass pipettes were loaded with a small volume of amphotericin B-free or gramicidin-free pipette solution, and backfilled with amphotericin B (100 μg/ml) (Santos et al., 2007) or gramicidin (2.5-5 μg/ml) (Park et al., 2012) containing solution. After cell attachment, access resistance was monitored and experiments were begun when the resistance < 100 MΩ, the resting membrane potential reached a stable level < -50 mV. Recordings were controlled by an EPC-10 amplifier combined with Pulse Software (HEKA Electronik) and analyzed using Igor Pro 6 (Wavematrics) and Origin Software (OriginLab). For *in vitro* optogenetic experiments, blue light (473 nm laser illumination (10 mW, 0.1-1 ms, Blue Sky Research, Milpitas, USA)) was delivered through a 40X water-immersion microscope objective. Light induced EPSCs ($EPSC_L$s) were first elicited at a frequency of 0.033 Hz (2 times/min). Monosynaptic or polysynaptic $EPSC_L$s were further differentiated by 0.2 Hz, 20 times light stimulation. We classified a connection as monosynaptic if the EPSC jitter (standard deviation of the light-induced $EPSC_L$s latency from stimulation) was < 1.6 ms (Cui et al., 2016; Doyle and Andresen, 2001; Wang and Zylka, 2009). Note that because bafilomycin A1 increases the incidence of release failure and jitter, the criteria used to differentiate mono- and polysynaptic responses, some monosynaptic responses may look polysynaptic, and some polysynaptic responses may look nonresponsive in these recording conditions. NBQX (20 μM), AP5 (50 μM), TTX (1 μM) and 4-AP (4 mM) were added into the recording solution for some experiments.

Reverse Transcription Polymerase Chain Reaction (RT-PCR)

Dissociated DRG cells (Dong et al., 2017; Fleming et al., 2015) or the cytosol of recorded spinal cord cells were gently transferred to an 8-well PCR reaction tube containing RT mix (1 μl RNaseOUT, 1.5 μl dNTPs and 1.5 μl oligo$(dT)_{20}$). Complementary DNA (cDNA) was synthesized using the SuperScript First-Strand Synthesis system (Invitrogen, 11904018). PCR was performed on cDNA with primers for *Vglut1* (5'-GCAGGAGGAGTTTCG
GAAG-3' and 5'-ACAATGGCAAAGCCAAAGAC-3', PCR product length=444), *Vglut2* (5'-GGAGAAGAAGCAGGACAACC-3' (exon 2) and 5'-TAGCCCCAGAAGAACGATCC-3' (exon 3), PCR product length=312 or 5'-GGGGAAAGAGGGGATAAAGA-3' (exon 1) and 5'-CTGCAGATGGGATCAGCATA-3' (exon 4), PCR product length=485), *Vglut3* (5'-TGTGTCATGGGTGTGAGGAT-3' and 5'-TGA TGGCATAGACAGGCAAG-3', PCR product length=409), *Grp* (5'-TCCTGGCTAAGATGTATCCG-3' and 5'-AGTCTACCAACT TAGCGGTTTG-3', PCR product length=294), *Grpr* (5'-ACTGTCAGCTGACAGGTACAAAG-3' and 5'-TAGGCACTCTGAATCA GATTTC-3', PCR product length=327) *Nmbr* (5'-CAACCTCTCCTTTCCCACAG-3' and 5'-GTCCATGGGGTTCACGATAG-3', PCR product length=430), and *Gapdh* (5'- GGTGAAGGTCGGTGTGAACG-3' and 5'-CTCGCTCCTGGAAGATGGTG-3', PCR product length=233).

Itch Behavior Assays

Itch behavior assays were conducted as previously described (Dong et al., 2017; Liu et al., 2012). The cheeks and nape were shaved one to three days prior to experiments. Mice were then placed in clear plexiglass behavioral boxes for at least one hour for two days for acclimation. Before testing, mice were acclimated to the testing chamber for at least 20 min, then blue light (5-25 mW, 2 s, 20 Hz) was given to the cheek, nape, and hind paw for 10 trials. Scratching (hind paw directed toward the area of injection), ipsilateral hind paw lifting (urge to scratch), head shaking, unilateral forepaw wiping, and bilateral forepaw wiping responses were counted. To determine pruritogen-induced itch behavior, chloroquine (8 mM, Sigma, C6628), histamine (100 mM, Sigma, H7250), SLIGRL (2 mM, R&D Systems, 1468), BAM8-22 (100 μM, R&D Systems, 1763), and 5-HT (2 mM, Sigma, H9523) were injected intradermally into either the cheek (10 μl) or the nape of the neck (50 μl) of the mouse, and scratching behaviors were observed for 20 min. A contact dermatitis model (Qu et al., 2014; Scott et al., 2002; Zhu et al., 2017) was produced by treating the skin with an allergen squaric acid dibutyl ester (SADBE, 25 μl, 1% in acetone, Sigma, 3339792) (Figure S5F). On days 3-5, SADBE was applied to the shaved abdomen once a day to initiate T lymphocyte sensitization. On days 13–17, SADBE was applied to the shaved nape skin to induce dermal inflammation and spontaneous scratching. On day 18, spontaneous scratching behavior was recorded for 30 minutes.

High-Speed Imaging

To capture various sub-second behavioral outcomes of mice after peripheral light-stimulation, we used a high-speed camera (FASTCAM UX100 800K-M-4GB - Monochrome 800K with 4GB memory) with an attached zoom lens (Nikon Zoom Wide Angle Telephoto 24-85mm f2.8) on a tripod as previously described (Abdus-Saboor et al., 2019). Behaviors were recorded at 500 frames per second (fps) with a resolution of 1024 x 576. To improve the imaging sensitivity of the camera, a far red-shifted LED light that mice cannot detect was also placed ~3 feet away from the Plexiglass chambers. Mice were acclimated on an elevated wire-mesh platform (Ugo Basile, Italy) for 1 h daily in transparent rectangular Plexiglas chambers (11.5 x 4.5 x 4 cm) for 3 days after shaving the cheek and nape. On the day of the experiment, they were habituated for ~45 min before peripheral 473 nm blue light (Shanghai Laser and Optics Century, BL473T8-150FC/ADR-800A) stimulation (5-25 mW, 20 Hz sine wave for 2-3 s, 10 trials with an inter-trial interval of 2-3 m)

was applied. Light stimulation and high-speed recording were triggered simultaneously when mice were completely calm without showing any movement. All videos were collected on a Dell laptop with Photron FASTCAM Viewer (PFV) software.

Mechanosensitivity and Thermal Sensitivity Behavior Assays

For the static mechanical sensitivity assay, mice were habituated for 2 days in the behavioral room. Under Plexiglas chambers, they were kept over a perforated wire mesh platform (Ugo Basile, Italy) which had 5 × 5 mm gaps, for ~45 min before starting the experiment. Paw withdrawal threshold was assessed using the up-down method (Chaplan et al., 1994). 8 calibrated and logarithmically spaced von Frey monofilaments (bending forces: 0.008, 0.02, 0.04, 0.07, 0.16, 0.4, 0.6 and 1 g; Stoelting, Wood Dale, IL) were selected to apply to the plantar hind paw. These were applied perpendicularly to the plantar surface with enough force to cause a slight buckling of the filament. First, the middle filament (0.16 g) was applied to the hind paw for 4-5 s. If the mouse responded with a withdrawal, an incrementally lower filament was applied. In the absence of withdrawal, an incrementally higher filament was applied. Trials were separated by at least 3-4 m to avoid sensitization and learning. A positive response was characterized as a rapid withdrawal of the paw away from the stimulus fiber within 4-5 s (Flicking or licking of the stimulated paw). Testing was continued until four filaments were applied (heavier or lighter, depending on the exact filament size to which the last response occurred) after the first one that produced a withdrawal. The final value of 50% withdrawal threshold was obtained by using pseudo-log calculator software in Excel which uses the following equation (Chaplan et al., 1994):

$$50\%\ \text{withdrawal threshold (g)} = (10[Xf + k\delta])/10{,}000$$

Where Xf = value (in log units) of the final von Frey filament used; k = tabular value for the pattern of positive/negative value and δ = mean difference (in log units) between stimuli. To examine dynamic mechanical hypersensitivity, sensitivity was measured by lightly stroking the lateral side of each hind paw from heel to toe with a paintbrush (#5/0) (Cheng et al., 2017). Brief paw lift (~1 s) were given the score 0. Score 1 was given for sustained lifting (more than 2 s) of the stimulated paw or a single gentle flinch of the stimulated paw; score 2 was given for a strong lateral hind paw lift above the level of the body or a startle-like jumping; and score 3 was given for multiple flinching responses or licking of the affected paw. The stimulation was repeated for three times at intervals of at least 3-4 min, and the average score for each mouse was obtained. For the constant temperature hot plate test, mice were placed on top of a hot plate (IITC, Life Science), preset to 50°C. The latency to response as determined by either licking of the hind paw or jumping was noted. Three trials at intervals of at least 15 min were taken and the average score for each mouse was obtained. In order to avoid injury to the mice, a cutoff of 30 s was set. The incremental hot plate test was carried out with the same apparatus as the constant temperature hot plate test. The initial plate temperature was set to 28°C and increased by 6°C/min towards a final temperature of 55°C (Alshahrani et al., 2012). The temperature when the first hind paw lick occurred was recorded. If no hind paw lick was observed, the test was terminated at 55°C. Three trials at intervals of at least 15 min were taken and the average score for each mouse was obtained. For the Hargreaves plantar test, animals were placed in Plexiglas chambers over the glass surface of the Hargreaves apparatus (UCSD Instruments, San Diego, CA, USA), and allowed to acclimate for about 45 min. A thermostat was used to check the constant temperature of the glass plate (~25°C). The heat stimulus was applied from a bulb beneath the glass, to the middle of the plantar surface. Paw flicking or licking in response to the stimuli was considered a positive response. Cutoff time was 20 s. The latency period (in sec.) was determined in three trials at intervals of ~10 min and the average obtained. To test cold sensitivity, mice were placed in Plexiglas chambers on a 2.54 mm thick elevated glass plate and allowed to habituate for at least 45 min. A dry ice pellet (1 cm) was applied to the lower glass surface underneath the hind paw of the animal, and the withdrawal (flick, lick, or both) latency in response to the dry ice-induced cooling of the glass surface area was measured. Each hind paw was tested three times with at least 15 min in between two consecutive stimulations. To avoid tissue damage, the cutoff latency was set to 10 s.

Image Acquisition

Images were collected using a Leica SP5II confocal microscope (fluorescent), Leica DM5000B microscope (bright field with a Leica DFC 295 camera and fluorescent with a Leica 345 FX camera), or a Nikon TE2000E microscope (fluorescent). Image manipulation and figure generation were performed in Fiji and Adobe Illustrator.

QUANTIFICATION AND STATISTICAL ANALYSIS

Cell number counting was performed in Fiji. Column graphs, line graphs, and pie charts were generated in GraphPad Prism 7. All data were reported and represented in column and line graphs as mean ± SEM. Sample sizes for histology and behavior experiments represent number of animals, while sample sizes for physiological recordings represent number of cells. Sample sizes and other statistical details are defined in figure legends and in the main text. Statistical significance was analyzed in GraphPad Prism 7 using chi-square tests for synaptic input proportions and unpaired two-tailed Student's t tests for all other experiments. Formal tests were not used to assess data distributions for the Student's t test normality assumption.